REVIEW

Carbon Neutralization WILEY

Check for updates

Electrochemical alcohol oxidation reaction on Precious-Metal-Free catalysts: Mechanism, activity, and selectivity

Jiawei Shi¹ | Jun Ma¹ | Enze Ma¹ | Jing Li¹ | Yang Hu² | Liyuan Fan³ | Weiwei Cai¹

¹Hydrogen Energy Technology Innovation Center of Hubei Province, Faculty of Materials Science and Chemistry, China University of Geosciences, Wuhan, Hubei, China ²Department of Energy Conversion and Storage, Technical University of Denmark, Lyngby, Denmark ³College of Science and Engineering, James Cook University, Townsville, Australia

Correspondence

Weiwei Cai, Hydrogen Energy Technology Innovation Center of Hubei Province, Faculty of Materials Science and Chemistry, China University of Geosciences, Wuhan 430074, Hubei, China.

Email: caiww@cug.edu.cn and willcai1985@gmail.com

Funding information

National Natural Science Foundation of China, Grant/Award Number: 22179121; Knowledge Innovation Program of Wuhan-Basic Research, Grant/Award Number: 2022010801010202; Research Fund Program of Guangdong Provincial Key Laboratory of Fuel Cell Technology, Grant/Award Number: FC202201

Abstract

The electrochemical alcohol oxidation reaction (AOR) is pivotal for the development of sustainable energy. The complete oxidation of alcohols has attracted extensive attention as a vital process in fuel cells. Moreover, as an alternative reaction to the oxygen evolution reaction, the selective oxidation of alcohols emerges as an effective means to lower the energy expenditure associated with electrolytic hydrogen production while yielding high-value products. Nonprecious metal materials have been widely applied in the selective oxidation catalysis of alcohols due to their cost-effectiveness and excellent durability. In recent years, leveraging the advantages of nonprecious metal materials in electrocatalytic AOR, researchers have delved into catalytic mechanisms and various efficient catalysts have been fabricated and evaluated. This review provides an overview of the current advancements in the electrocatalytic selective oxidation of diverse alcohols and the catalytic systems centered around nonprecious metal materials. It systematically summarizes the shared traits and distinctions in catalytic reaction characteristics across various systems, thereby laying the theoretical foundation for developing novel catalyst systems that are efficient, stable, and highly selective. This review will facilitate the utilization of nonprecious metal catalysts further toward the electrocatalytic oxidation of alcohols.

KEYWORDS

activity, electrochemical alcohol oxidation reaction, mechanism, Precious-Metal-Free catalysts, selectivity

INTRODUCTION 1

Enhancing the hydrogen energy cycle to achieve the widespread application of hydrogen on a large scale and to reshape the energy system structure is critical toward realizing zero-carbon emission.^[1] Within the hydrogen energy

cycle, hydrogen production stands as the critical starting point.^[2] A substantial portion of hydrogen production is still from fossil fuels, a practice with heavy carbon emissions.^[3] There is an imperative need to bolster the share of clean hydrogen.^[4] Among the various technologies for clean hydrogen production, water electrolysis

This is an open access article under the terms of the Creative Commons Attribution License, which permits use, distribution and reproduction in any medium, provided the original work is properly cited.

© 2024 The Authors. Carbon Neutralization published by Wenzhou University and John Wiley & Sons Australia, Ltd.

and-conditions) on Wiley Online Library for rules of use; OA articles are governed by the applicable Creative Commons License

WILEY- Carbon Neutralization

stands out with the most promising potential for practical applications, as shown. In Reaction $1^{[5]}$:

 $2H_2O \rightarrow 2H_2 + O_2$ (Reaction 1, Total reaction).

The following equations illustrate the mechanism of the hydrogen generation in acidic electrolysis systems, Reaction 2–3:

 $4H^+ + e^- \rightarrow 2H_2$ (Reaction 2, Cathode hydrogen evolution reaction);

 $2H_2O \rightarrow 4H^+ + O_2 + 4e^-$ (Reaction 3, Anode oxygen evolution reaction).

And in alkaline electrolysis systems, reaction $(4-5)^{[6]}$:

 $4H_2O + 4e^- \rightarrow 2H_2 + 4OH^-$ (Reaction 4, Cathode hydrogen evolution reaction);

 $4OH^- \rightarrow 2H_2O + O_2 + 4e^-$ (Reaction 5, Anode oxygen evolution reaction).

The anodic half-reaction of electrolytic hydrogen production is the oxygen evolution reaction (OER), with a theoretical oxygen evolution potential of 1.229 V.^[7] It is a multielectron reaction with slow kinetics requiring high energy input. [8] A comprehensive technical and economic assessment reveals that OER accounts for 95% of the total electricity consumption during water electrolysis for hydrogen production.^[9] Consequently, this high energy demand significantly elevates the costs associated with electrolytic hydrogen production and is the major impediment to its widespread application. [10] In addition to the pursuit of designing and synthesizing efficient and durable OER catalysts, [11] an alternative avenue to lower the cost has attracted more attention in recent years.^[12] Researchers have investigated certain organic small molecule electro-oxidation reactions that operate at lower potentials than the OER, thereby effectively reducing the energy consumption for hydrogen production. [13] Furthermore, owing to the inherent efficiency of electrocatalysis, products with higher intrinsic value than oxygen, such as formic acid, can be efficiently generated at the anode, further contributing to the total benefit of hydrogen production. [14] The most well-studied electrolytic hydrogen production system is the alkaline electrolysis system, [15] considering solubility, stability, raw material cost, and product value. Moreover, the stringent requirements of industrial-grade hydrogen production, such as high current density, reasonable cost, excellent durability and stability, and nonprecious metals-based catalytic systems, emerge as the preferred option. [16]

Various small molecule oxidation reactions have been proposed as alternatives to the OER. [17] The alcohol

(methanol, [18] ethanol, [19] glycerol, [20] etc.) oxidation reaction (AOR) has emerged as a promising method and drawn much attention among researchers due to the ready availability and cost-effectiveness of alcohol feedstocks and the high value of carboxylic acid oxidation products. [21] Additionally, the high solubility and stability of small alcohol molecules in electrolytic environments hold the potential to achieve a high current density for industrial-scale hydrogen production. The concept of alcohol oxidation for hydrogen generation within methanol-water electrolysis systems was introduced in 1947, albeit without significant progress. [22] However, in the 21st century, as hydrogen production from water electrolysis becomes promising, AOR has also experienced a remarkable acceleration. [23] Compared with the high cost and limited stability associated with precious metal catalysts, nonprecious metal AOR catalysts present distinct advantages in affordability, durability, and other key factors. [24] In recent years, researchers have increasingly recognized the potential of nonprecious metal materials in the electrocatalytic AOR for electrolytic hydrogen production. [25] Numerous investigations have been conducted on the mechanisms underlying various AORs to engineer high-efficiency catalysts tailored to these processes. This comprehensive review delves into the mechanisms of how nonprecious metal catalysts facilitate AOR (Figure 1). [26] It consolidates the latest advancements and synthesis methodologies for electrocatalysts dedicated to various AORs. Additionally, the review explores and contrasts the application of AOR in different electrolysis

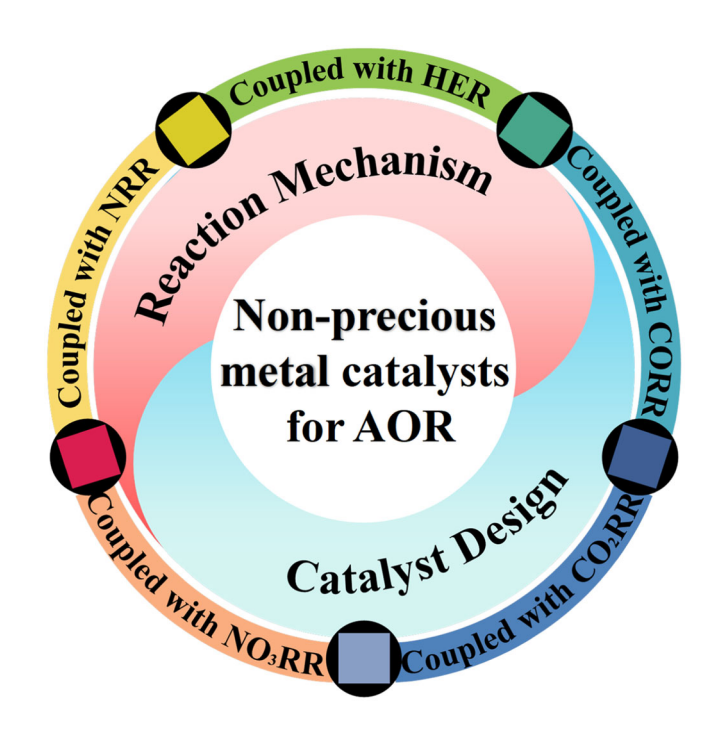


FIGURE 1 Overview of nonprecious metal materials used for electrocatalytic AOR.

27693335, 2024. 2. Downloaded from https://onlinelibtrary.wiley.com/doi/10.1002/cm2.116 by James Cook University. Wiley Online Library on [26/11/2025]. See the Terms and Conditions (https://onlinelibtrary.wiley.com/ems-and-conditions) on Wiley Online Library for rules of use; OA articles are governed by the applicable Creative Commons Licensed

systems, [27] such as coupled hydrogen evolution reaction (HER), [28] nitrogen reduction reaction (NRR), [29] nitrate reduction reaction (NO₃RR), [30] carbon oxide reduction reaction (CORR), [31] and carbon dioxide reduction reaction (CO₂RR). An assessment of their potential and value is provided. Ultimately, this review aims to help readers better understand AOR and furnish valuable insights into the development of efficient AOR catalysts and their integration into electrolytic systems.

2 | AOR MECHANISM

As hydrogen production via overall water electrolysis (OWE) gains increasing attention within hydrogen energy systems, the AOR is emerging as a viable alternative to the OER. As illustrated in Table 1, the theoretical oxidation potential of AOR is approximately 0.1 V, significantly lower than OER, thereby enabling the attainment of lower cell voltage for electrolytic hydrogen production. However, given that AOR entails a multielectron reaction characterized by sluggish kinetics, a catalyst is needed to catalyze the reaction. A comprehensive investigation into the AOR reaction mechanism holds the potential to facilitate the development of highperformance catalysts. [38] In recent years, substantial advancements in exploring the AOR reaction mechanism, particularly concerning nonprecious metal catalytic materials, have been reported. [39] Researchers have proposed various reaction mechanisms, including the nucleophile oxidation reaction mechanism (NOR), the surface adsorption mechanism (SAM), and the lattice oxygen participation mechanism (LOM).

2.1 | NOR mechanism

Alcohol molecules are characterized by nucleophilic functional groups, namely hydroxyl groups. Hence, the AORs can be categorized as a NOR. Wang and his research team have introduced a classic two-step reaction

mechanism for the NOR reaction involving Ni-based materials, as shown in Figure 2a. [40] To clarify the structural evolution and mechanism involved, β-Ni (OH)2, known for its distinct characteristics in OER reactions, was selected as the model catalyst. Ethanol oxidation reaction (EOR) served as the model reaction. The NOR mechanism was identified through electrochemical impedance spectroscopy (EIS), in-situ Raman, and in-situ X-ray absorption spectroscopy (XAS). During the NOR process, potentials from 1.35 to 1.45 V were applied. It was observed that high-frequency interface reactions were exclusive at elevated current densities. This observation validates that NOR transpires at the high-frequency interface between diffuse double layer (DDL) and β-Ni (OH)₂. A low-frequency interface reaction emerges as the NOR process progresses beyond 1.50 V. Subsequently, after exceeding 1.60 V, the catalyst surface becomes passivated, as indicated by the appearance of a secondhalf semicircle in the second quadrant of the Nyquist diagram. Corresponding to the LSV curve of β -Ni(OH)₂, a distinct passivation trend becomes evident after 1.50 V during the NOR process (Figure 2c). Consequently, in the case of β-Ni(OH)₂, NOR primarily takes place at the high-frequency interface situated between β-Ni(OH)₂ and DDL. Notably, the NOR activity at the low-frequency interface is significantly lower, leading to a passivation beyond 1.50 V during the NOR process. A comprehensive analysis, encompassing the equivalent resistance and electrical potential, elucidates the dynamic changes in high-frequency and low-frequency interface reactions of β-Ni(OH)₂ under various electric potentials.

Subsequent studies have been conducted by numerous researchers, affirming that the NiOOH generated through the electro dehydrogenation of Ni-based materials serves as the catalytically active site for AOR. [41] The formation and reduction of NiOOH to Ni(OH)₂ represent pivotal steps in the AOR catalytic process, with the consumption of NiOOH occurring rapidly. [42] In situ Raman spectroscopy has been employed to confirm that AOR significantly inhibits the generation of NiOOH in Ni-based catalysts, thus supporting the NOR mechanism. [43]

TABLE 1 The theoretical voltages (U_{cell}^0) for the electrolysis of representative substances.

Substances	Reaction equation	${ m U^0_{ cell}/V}$	Reference
Water	$2H_2O \rightarrow 2H_2 + O_2$	1.229	[33]
Methanol	$CH_4O + H_2O \rightarrow 3H_2 + CO_2$	0.016	[34]
Ethanol	$C_2H_6O + 3H_2O \rightarrow 6H_2 + 2CO_2$	0.084	[35]
Ethylene glycol	$C_2H_6O_2 + 2H_2O \rightarrow 5H_2 + 2CO_2$	0.026	[22]
Glycerol	$C_3H_8O_3 + 3H_2O \rightarrow 7H_2 + 3CO_2$	0.0029	[36]
Benzyl alcohol	$Ph-CH_3O + H_2O \rightarrow 2H_2 + Ph-CO_2H$	0.48	[37]

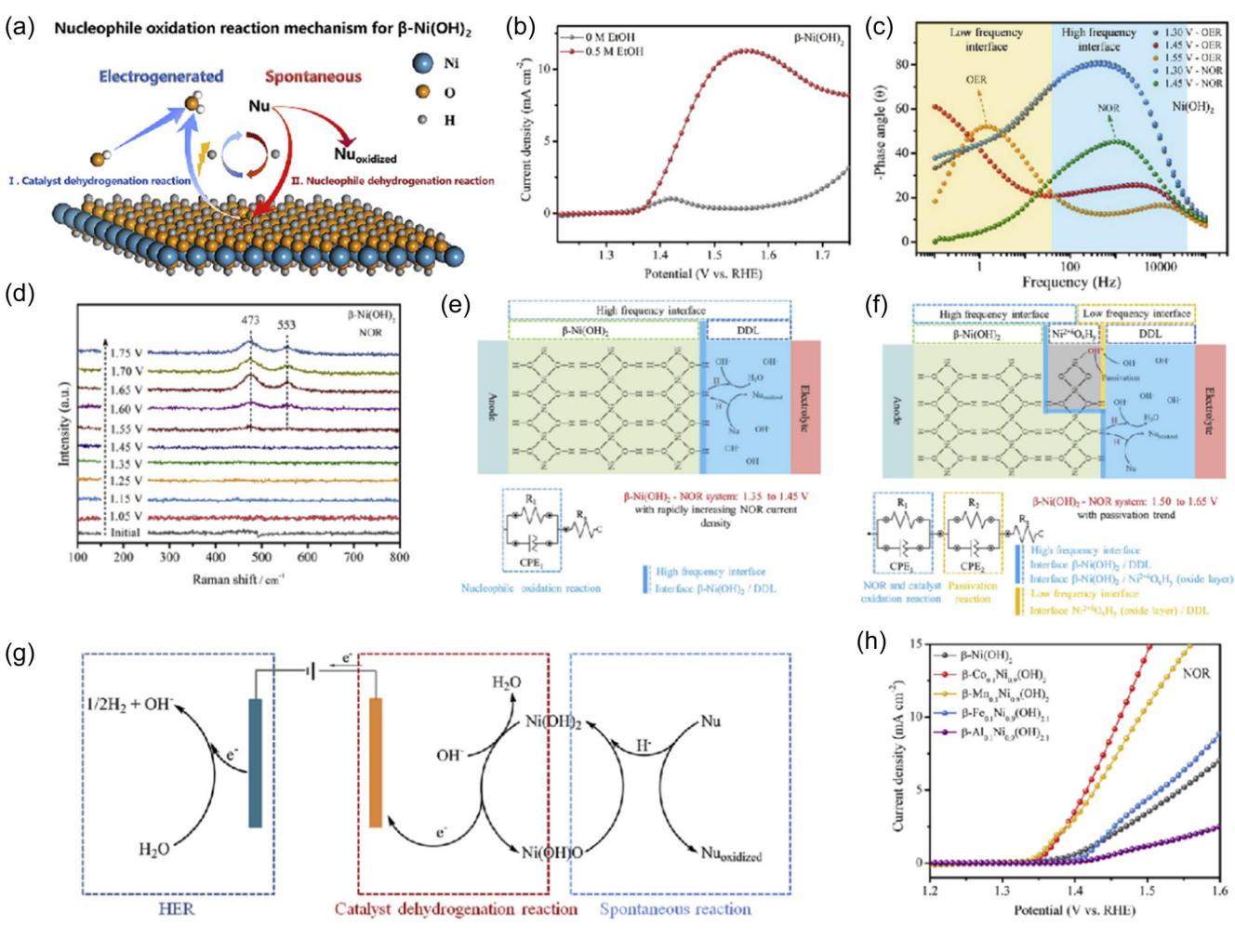


FIGURE 2 (a) Nucleophile oxidation reaction mechanism of β-Ni(OH)₂; (b) LSV (5 mV s⁻¹, without iR-correction) for β-Ni(OH)₂ on GCE in 1 M KOH with/without 0.5 M ethanol; (c) Bode plots of β-Ni(OH)₂ electrode for OER and NOR in different potentials; (d) In-situ Raman spectroscopy of β-Ni(OH)₂ electrode for NOR; (e) R(QR) model in NOR system from 1.35 to 1.45 V; and (f) R(QR)(QR) model in NOR system from 1.50 to 1.65 V; (g) Proposed NOR mechanism scheme for β-Ni(OH)₂; (h) 1 M KOH with 50 mM ethanol, β-M_{0.1}Ni_{0.9}(OH)_x (M = Co, Mn, Fe, and Al) in 1 M KOH with 50 mM ethanol. Reproduced with permission: Copyright 2020, Cell Press. [40]

In the context of EIS analysis, the high-frequency interface between β-Ni(OH)₂ and DDL exhibits greater clarity than the low-frequency interface. To enhance the understanding of the low-frequency interface, in-situ Raman spectroscopy was employed (Figure 2d). Within the NOR system, the occurrence of NOR at the high-frequency interface between β-Ni(OH)₂ and DDL is confined to the potential range of 1.35 to 1.45 V. In this scenario, the surplus electrons of nucleophiles and protons efficiently and promptly replenish the hydrogen vacancies in β-Ni(OH)O, denoted as β -Ni(OH)O + H_{Nu} + e⁻_{Nu} = β -Ni(OH)₂. Consequently, the morphology and electronic structure of β-Ni (OH)₂ remain unaltered without any phase transitions, as depicted in Figure 2e. Subsequent to 1.50 V in the NOR system, the electron transfer rate for the dehydrogena tion reaction of catalyst $(\beta-Ni(OH)_2 + OH^- = \beta-Ni(OH)$ $O + H_2O + e^-$) takes effect. These findings provide compelling evidence that, for β -Ni(OH)₂, NOR activity emanates from the β -Ni(OH)O intermediate rather than Ni^{2+ δ}O_vH_v or OER intermediates.

27693325, 2024, 2, Downloaded from https://onlinelibrary.wiley.com/doi/10.1002/cnl2.116 by James Cook University, Wiley Online Library on [26/11/2025]. See the Terms and Conditions (https://onlinelibrary.wiley.com/

and-conditions) on Wiley Online Library for rules of use; OA articles are governed by the applicable Creative Commons License

Time-of-flight secondary ion mass spectrometry (TOF-SIMS) is a valuable test for tracing labeled hydrogen isotopes in nucleophiles throughout the NOR process. Whether NOR is initiated directly or nucleophiles are introduced midway, it is not feasible to detect β-Ni(OH)O at the potential of 1.095 V. This observation substantiates the notion that, in the case of β -Ni(OH)₂, the nucleophile dehydrogenation reaction occurs spontaneously. Consequently, the NOR mechanism for β -Ni(OH)₂ is a two-step, one-electron reaction. This mechanism includes the electrogenerated catalyst dehydrogenation reaction and the spontaneous nucleophile dehydrogenation reaction. In the initial step, the OH $^-$ couples with the proton of β -Ni (OH)₂ and is released as H₂O. Simultaneously, electrons

are transferred within the circuit, creating β -Ni(OH)O featuring electrophilic oxygen. In the subsequent step, the electrophilic oxygen of β -Ni(OH)O autonomously and rapidly abstracts electrons and protons from the nucleophile. This process leads to the conversion of β -Ni(OH)O into β -Ni(OH)₂, as illustrated in Figure 2g. It is important to note that when the reaction rate of the second step considerably exceeds that of the first step, β -Ni(OH)₂ theoretically remains unchanged. This is because the accumulation of the β -Ni(OH)O intermediate is avoided, preventing any phase transitions. Consequently, under an appropriate potential, an excess of nucleophiles maintains the morphology, crystal structure, and surface electronic state of β -Ni(OH)₂ during the NOR process.

Through verification experiments and density functional theory (DFT) calculations, distinct NOR pathways for β -Ni(OH)₂ and NiO are postulated. The NOR activity originates from β -Ni(OH)O with electrophilic lattice oxygen and NiO(OH)_{ads} with electrophilic adsorbed oxygen. The transition between β -Ni(OH)₂ and β -Ni(OH)O acts as an intermediate step in the NOR process, and its relationship to the crystal structure of hydroxide is direct. By adjusting the lattice oxygen ligand environment of β -Ni(OH)₂ through moderate doping with Co²⁺ or Mn²⁺, the transfer of lattice hydroxyl groups in β -M_{0.1}Ni_{0.9}(OH)₂ to β -M_{0.1}Ni_{0.9}(OH) O is effectively reduced, thereby enhancing NOR activity (Figure 2h).

2.2 | SAM

For nickel-based catalysts, the nickel hydroxide formed by in-situ reconstitution is often considered the source of alcohol electrooxidation. Feng and colleagues have proposed a recycling pathway based on experimental and computational research. [9] This pathway involves a reversible redox transformation of Ni^{II}(OH)₂/Ni^{III}-OOH in conjunction with the methanol oxidation reaction (MOR), as shown in Figure 3a,b. This process creates a cooperative active site that includes Ni^{III} and neighboring electrophilic oxygen species, which work together to facilitate spontaneous and nonspontaneous MOR processes. This bifunctional mechanism provides a sound explanation for the formation of highly selective formate and the transient presence of Ni^{III}-OOH. Using operational spectroscopy techniques, researchers have observed the transient and limited formation of Ni^{III}-OOH in NiM-LDHs (Figure 3c,d). In MOR conditions, characteristic Ni^{III}-O bands become noticeable at $1.37\,V_{RHE}$ within the potential range of 1.37– $1.52\,V_{RHE}$. These characteristic bands are less prominent compared with the primary Ni^{II}-O band. As the applied potential

decreases from 1.52 to $1.12\,V_{RHE}$, the characteristic Ni^{III} -O bands gradually weaken and disappear. These observations indicate that Ni ions in NiMn-LDH undergo transformation between Ni^{II} and Ni^{III} during the MOR catalysis process. Meanwhile, the Mn^{III} -O band, at $600\,\mathrm{cm}^{-1}$, remains constant throughout the entire potential scan, suggesting that Mn ions in NiMn-LDH do not participate in the redox transition. DFT calculations reveal that (Figure 3e,f), in comparison to the NiFe model, the d band center of NiMn is closer to the Fermi level. This indicates a stronger OH^- adsorption on the NiMn surface, verifying the lower ΔG_{OX} relative to the NiFe model.

Wang et al. proposed a surface adsorption catalytic mechanism that circumvents NiOOH conversion. [44] The $MoO_3/Ni(OH)_2$ catalyst can directly catalyze MOR by incorporating Mo^{6+} into $Ni(OH)_2$, thus bypassing the NiOOH process. Theoretical calculations indicate that Ni^{2+} serves as an adsorption site for methanol, and the doped Mo^{6+} plays a crucial role in capturing deprotonated H·. Thanks to the synergistic effect of Mo and Ni, the energy barrier of the $CH_2O^* \rightarrow CHO^* + H^*$ process is significantly reduced (from 1.52 to -0.03 eV), preventing the formation of NiOOH.

2.3 | LOM

Sounak Roy and colleagues extensively investigated the mechanism of $\text{La}_{2-x}\text{Sr}_x\text{NiO}_{4+\delta}$ oxides for MOR. They discovered that the electronic properties induced by structural deformations and oxygen defects are attributed to lipoprotein doping in the A site. Optimal Sr^{2+} doping in $\text{La}_{1.4}\text{Sr}_{0.6}\text{NiO}_{4+\delta}$ results in a high degree of Ni^{3+} 3d-O 2p hybridization, with the O-2p center positioned very close to the Fermi level. This enhances conductivity and leads to Fermi level pinning at the top of the O 2p band, making the lattice oxygen in $\text{La}_{1.4}\text{Sr}_{0.6}\text{NiO}_{4+\delta}$ easily oxidizable. Building upon these empirical and theoretical findings, a proposed mechanism for oxygen vacancy-induced lattice oxygen-mediated MOR is developed. [45]

Inspired by the remarkable OER performance achieved through lattice oxygen activation, Xu and their team synthesized a range of catalysts featuring various O-2p band center levels, including LaCoO₃, SrCoO_{3- σ}, FeO_xH_y, and NiO_xH_y. ^[46] The local atomic structure of the central metal ions (Co in LaCoO₃ and SrCoO_{3- σ}, Fe in FeO_xH_y, and Ni in NiO_xH_y) was scrutinized through K-edge X-ray absorption near-edge structure (XANES) and extended X-ray absorption fine structure (EXAFS) analyses. As revealed by the XANES spectrum, the valence states of Co, Fe, and Ni are determined to be +3, +3, and +2, respectively. Notably,

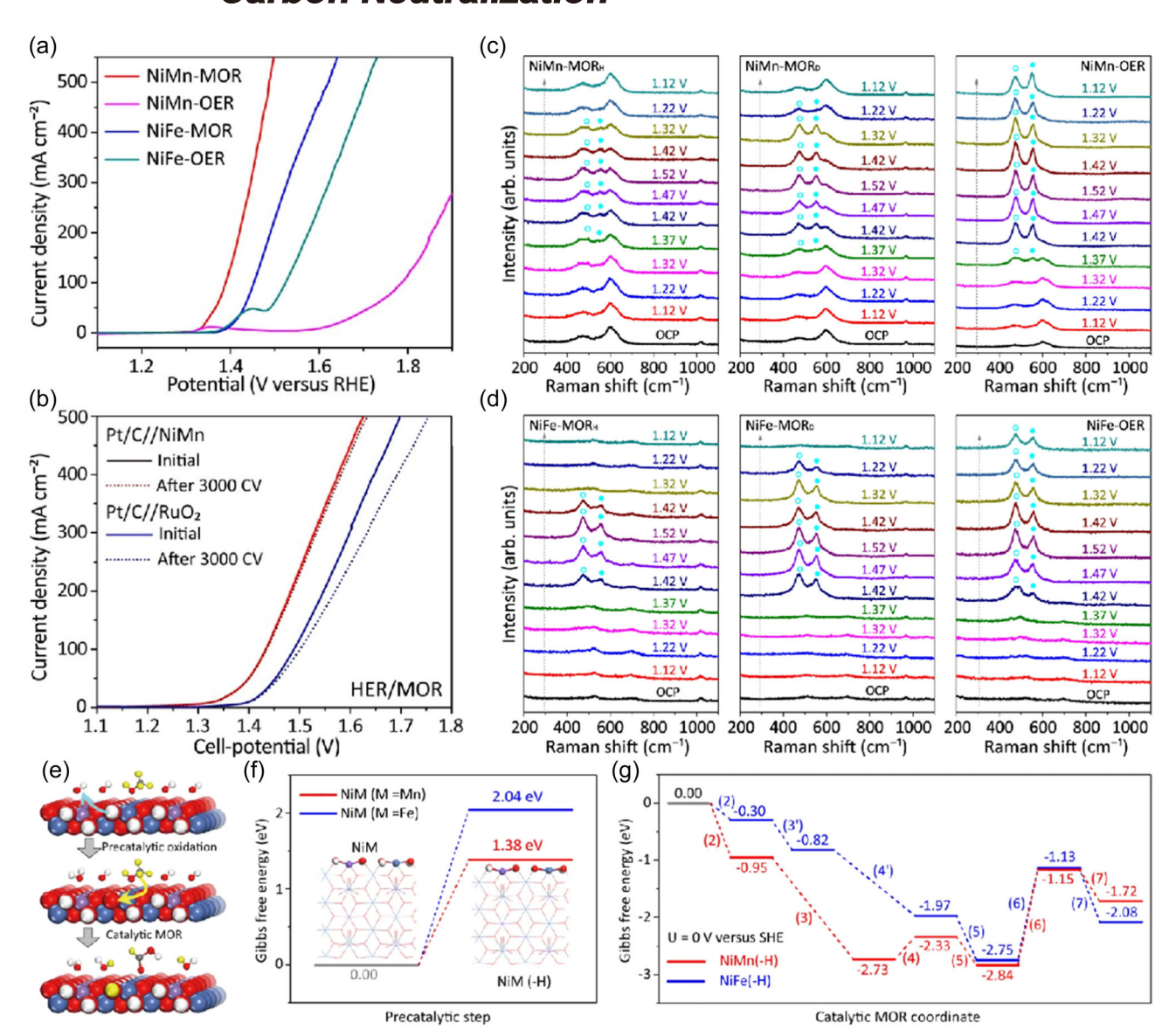


FIGURE 3 (a) The LSV curves of NiMn and NiFe-LDHs both recorded in 1 M KOH without and with 3 M CH₃OH (with iR-correction); (b) Cell LSV curves (without iR-correction) of HER/MOR electrolysis; Operando Raman spectra of (c) NiMn and (d) NiFe-LDHs both obtained at various potentials under optimal MOR (the subscript H or D denotes CH₃OH/H₂O or CD₃OD/D₂O solution) and OER conditions; (e) Reaction scheme for the overall MOR on NiM-LDHs (M=Mn, Fe); Gibbs free energy diagrams for the (f) precatalytic process and (g) catalytic MOR process. Reproduced with permission: Copyright 2023, Nature.^[9]

the coordination number of $SrCoO_{3-\sigma}$ is marginally smaller than that of $LaCoO_3$, and the peak intensity at 1.4 Å is somewhat diminished.

By employing an ¹⁸O isotope-labeled catalyst, it was ascertained that the oxygen atoms within the formate generated during the electrocatalytic MOR could trace their origin back to the lattice oxygen of the catalyst (Figure 4a). The O-2p band center level was established as a potent descriptor for predicting the catalytic performance of the catalyst, encompassing formate yield and Faradaic efficiency. Gas chromatographymass spectrometry (GC-MS) measurements underscore that lattice oxygen actively engages in the

reaction for highly covalent catalysts like $SrCoO_{3-\sigma}$ and NiO_xH_y . Conversely, for less covalent materials such as $LaCoO_3$ and FeO_xH_y , lattice oxygen remains uninvolved. As illustrated in Figure 4b, the O-2p band centers of $SrCoO_{3-\sigma}$ and NiO_xH_y are closer to the Fermi level than $LaCoO_3$ and FeO_xH_y . When the O-2p state of the catalyst approaches the Fermi level closely (near the redox potential of O_2/H_2O), it renders the participation of lattice oxygen thermodynamically favorable. Consequently, the elevation of the O-2p band may be the underlying physical rationale for lattice oxygen's involvement in the methanol electro-oxidation reaction.

27693325, 2024, 2, Downloaded from https://onlinelibrary.wiley.com/doi/10.1002/cn12.116 by James Cook University, Wiley Online Library on [26/11/2025]. See the Terms

ns) on Wiley Online Library for rules of use; OA articles are governed by the applicable Creative Commons License

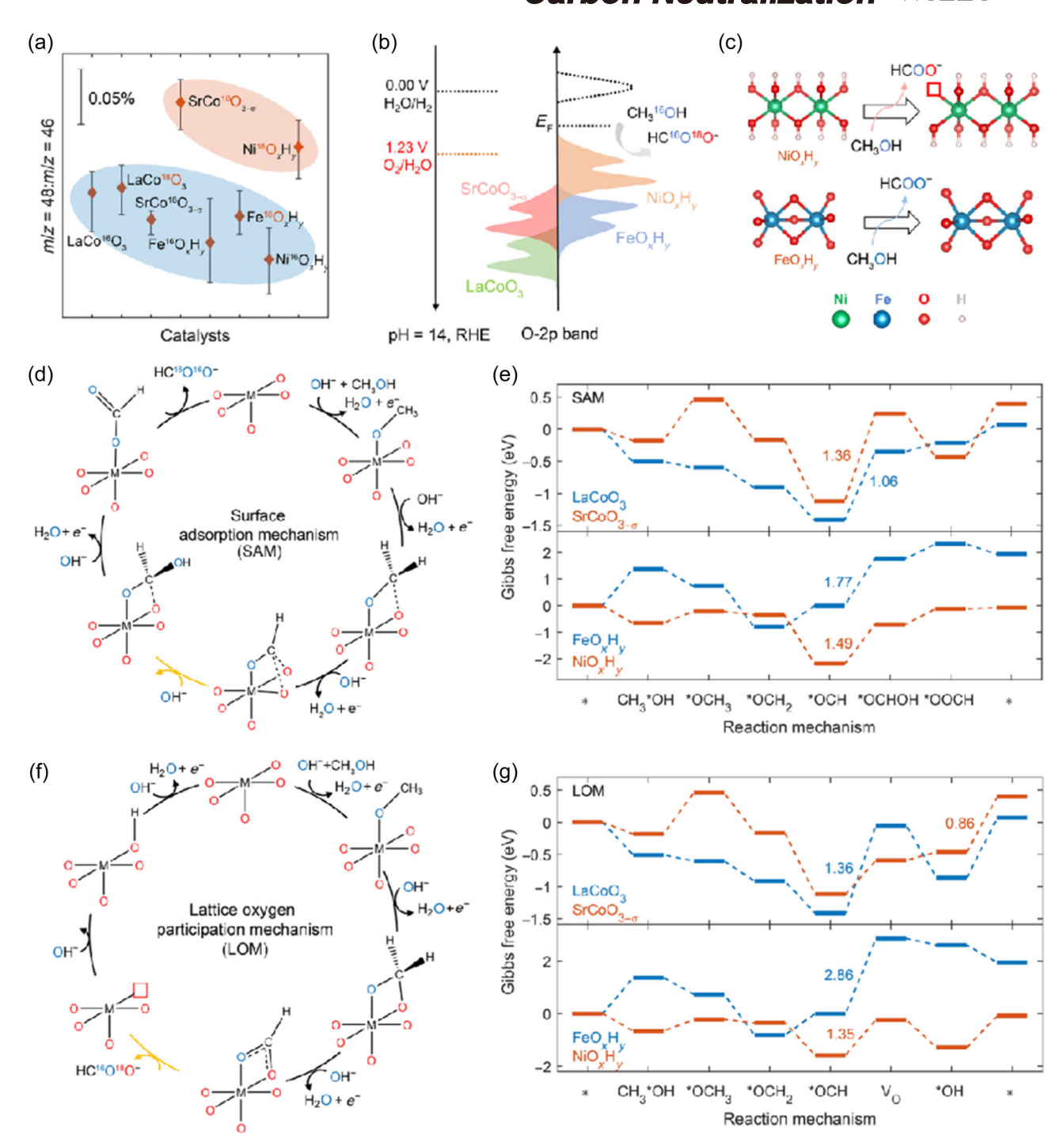


FIGURE 4 (a) HC¹⁶O¹⁸OH/HC¹⁶O¹⁶OH ratios of ¹⁸O-labeled catalysts (LaCo¹⁸O₃, SrCo¹⁸O_{3-σ}, Fe¹⁸O_xH_y, and Ni¹⁸O_xH_y) in contrast with unlabeled comparisons; (b) Schematic band diagrams of LaCoO₃, SrCoO_{3-σ}, FeO_xH_y, and NiO_xH_y; (c) Different reaction diagrams between NiO_xH_y and FeO_xH_y; (d) Possible reaction mechanisms for SAM and (e) Computed free energy changes for the SAM; (f) Possible reaction mechanisms for LOM and (g) Computed free energy changes for the LOM. Reproduced with permission: Copyright 2023, AAAS. ^[46]

Through the involvement of lattice oxygen, demonstrated through the isotopic labeling experiment in Figure 4a, $SrCoO_{3-\sigma}$ and NiO_xH_y , characterized by higher O-2p band center levels, exhibit a distinct methanol electrooxidation mechanism in contrast to $LaCoO_3$ and FeO_xH_y , as delineated in Figure 4c.

Specifically, this divergence manifests as a SAM and a LOM, shown in Figure 4d,f.

In the context of SAM, the initial three steps constitute a deprotonation process leading to the formation of a *CHO intermediate. Subsequently, two hydroxide attack steps follow, culminating in the generation of

HC¹⁶O¹⁶O⁻. In contrast, the first three steps in LOM also involve deprotonation processes. But with the shift of attacking species from OH⁻ to lattice oxygen, *¹⁶O¹⁸OCH is formed. After HC¹⁶O¹⁸O⁻ is released, an oxygen vacancy will be created. Consecutively, a proton-electron transfer step and a deprotonation step facilitate the regeneration of the metal-oxygen surface. Figure 4e,g summarizes the energy changes and diagrams for the two reaction pathways across the four catalysts.

Two salient features deserve attention: (i) LOM demonstrates a lower rate-determining step (RDS) energy for $SrCoO_{3-\sigma}$ and NiO_xH_v , while it exhibits a higher RDS energy for LaCoO3 and FeOxHy; (ii) The RDS energy for the LOM pathway on $SrCoO_{3-\sigma}$ and NiO_xH_v is notably lower than that of the SAM pathway on LaCoO3 and FeO_xH_v. These distinct behaviors were attributed to the differences in the O-2p band center levels, which have been established as effective indicators of the performance in the electrocatalytic MOR. Among all the catalysts investigated, NiO_xH_v possesses the highest O-2p band center level and consistently demonstrates an exceptional formate Faradaic efficiency, achieving nearly 100% over a wide range of current densities in membrane electrode assembly (MEA) assessments. This proposed catalytic mechanism for methanol electrooxidation, including lattice oxygen participation, effectively elucidates the relationship between the O-2p band center level and the formate production rate or the Faradaic efficiency of the catalyst.

2.4 | C-C bond cleavage mechanism of polyhydric alcohols

Polyhydroxy alcohols possess proximate hydroxyl groups, as exemplified by ethylene glycol and glycerol, whose predominant oxidation products predominantly manifest as formic acid. Consequently, the oxidation process involves not only the conversion of hydroxyl groups to carboxyl groups but also addresses the intricacies of C-C bond cleavage. Wang's team elucidated the NOR mechanism underlying the electrooxidation of primary alcohol/ vicinal diol on NiO.[47] This mechanism entails an electrochemical step, characterized by the generation of Ni³⁺-(OH)_{ads}, and a subsequent nonelectrochemical step, instigated by electrocatalysts, involving the spontaneous reaction between Ni3+-(OH)ads and nucleophiles. Within this mechanism, two distinct electrophilic oxygenmediated mechanisms (EOM) emerged, specifically EOM involving hydrogen atom transfer (HAT) and EOM involving C-C bond cleavage. These mechanisms assume pivotal roles in the electrooxidation processes, steering primary alcohols toward carboxylic acids and

ethylene glycol toward formic acid. Two categories of nonelectrochemical steps surfaced: those induced by electrocatalysts and those unrelated to electrocatalysts. Notably, the electrooxidation of alcohols on NiO unfolds as an indirect electrochemical reaction utilizing Ni³⁺-(OH)_{ads}, comprising both electrochemical steps (the production of Ni3+-(OH)ads) and electrocatalyst-induced nonelectrochemical steps (Ni3+-(OH)ads induced HAT and C-C bond cleavage). Consequently, the electrooxidation of alcohols on NiO demonstrates dual electrocatalytic functions: EOM involving HAT and EOM involving C-C bond cleavage. The synergistic interplay between these mechanisms, coupled with the participation of nonelectrochemical steps like hydration reactions, enables the electrochemical oxidation of R-CH2OH to R-COOH and R-CHOH-CH2OH to R-COOH and HCOOH on NiO.

Subsequently, the research team led by Wang et al. pursued an investigation into the oxygen/nickel oxyhydride species (NiO_xH_v) characterized by vacancy defects, which demonstrated heightened efficacy in electrocatalytic AOR. [48] They proffered a catalytic mechanism predicated on defect induction for AOR. In the case of defect-free β-Ni(OH)₂ catalyst, the exclusive redox medium comprises electrophilic lattice oxygen generated through electrooxidation. This medium solely facilitates hydrogen transfer reactions, such as the electrooxidation of primary alcohols into carboxylic acids, without the catalysis of C-C bond cleavage. Consequently, defect-free β-Ni(OH)₂ lacks the capability to propel electrooxidation reactions involving adjacent diols and C-C bond cleavage. The pivotal breakthrough comes with the introduction of an oxygen defect-induced adsorption oxygenmediated mechanism, enabling NiOxHv to catalyze the electrooxidation of adjacent diols, thereby yielding carboxylic acids and formic acids.

3 | AOR CATALYST DESIGN

Nonprecious metals are characterized by their abundance, widespread availability, and cost-effectiveness, making them essential components in various catalytic domains, including electrocatalytic alcohol oxidation. Among the nonprecious metal materials reported for their AOR catalytic activity are oxides, hydroxides, sulfides, borides, and others of Ni, Co, Fe, Cu, and more. [49] Researchers have successfully enhanced AOR catalyst performance through a range of strategic approaches. These methods encompass engineering, [50] heteroatom doping, heterojunction formation, [43] electron cloud regulation, [51] amplification of specific surface area, and optimization of conductivity. [52] Moreover, due to inherent distinctions in the structure, size, mass transfer rate, and solubility of various alcohol

27693325, 2024, 2, Downloaded from https://onlinelibrary.wiley.com/doi/10.1002/cnl2.116 by James Cook University, Wiley Online Library on [26/11/2025]. See the Terms and Conditions (https://onlinelibrary.wiley.com

and-conditions) on Wiley Online Library for rules of use; OA articles are governed by the applicable Creative Commons License

molecules, variations arise in their respective catalysts' conductivity, mass transfer, and other characteristics.

The design of AOR catalysts is based on the advancement of alkaline OER catalysts, primarily composed of Ni-based and Co-based materials. Strategies employed to enhance catalyst activity are generally universal, encompassing approaches such as defect engineering and hybridization. In recent years, as the understanding of the AOR mechanism has deepened, researchers have uncovered that the activity of AOR and OER catalysts is not entirely positively correlated. Cai et al. discovered that F can augment the catalytic activity of Ni, Fe layered double hydroxides (NiFe-LDH) for EOR, with marginal improvement in OER catalytic activity. [42] Wang et al. suppressed the catalytic activity of Ni(OH)2 on OER while enhancing its MOR catalytic performance through Mo doping.[44]

Catalysts for low-grade fatty 3.1 alcohols

3.1.1 **MOR**

Methanol, being the simplest alcohol, possesses the advantages of widespread availability and affordability. Its oxidation potential is 0.016 V, as indicated in Table 1, which is significantly lower than that of OER.[53] Incomplete methanol oxidation can be achieved by utilizing nonnoble metal catalysts, forming formic acid, a product with a higher added value. [54] Consequently, methanol oxidation represents an ideal alternative to OER, and it has emerged as one of the most extensively researched AORs. [55] Researchers have designed and synthesized highly effective MOR catalysts, employing various strategies such as heteroatom doping, anion coordination control, heterostructure assembly, defect optimization, and similar approaches. These strategies can potentially make the electrooxidation of methanol a more energy-efficient process with applications in both energy production and the chemical industry.^[56]

Wang and colleagues synthesized Ni-based materials employing different anions (NiPx, NiSx, and NiSex, shown in Figure 5a) to modulate the coordination of oxygen anions during the in-situ reconstruction of nickel oxyhydroxide. [57] Among these materials, NiOOH-PO_x displayed the most remarkable electrocatalytic activity for the selective oxidation of methanol into formic acid. This superior performance arises from the enhanced capacity for adsorbing OH* and methanol, which facilitates the formation of CH₃O* intermediates. Concurrently, the coordinated phosphate oxygen anion effectively finetunes the d-band center of the Ni site, enhances Ni-O covalency, and thereby bolsters catalytic activity.

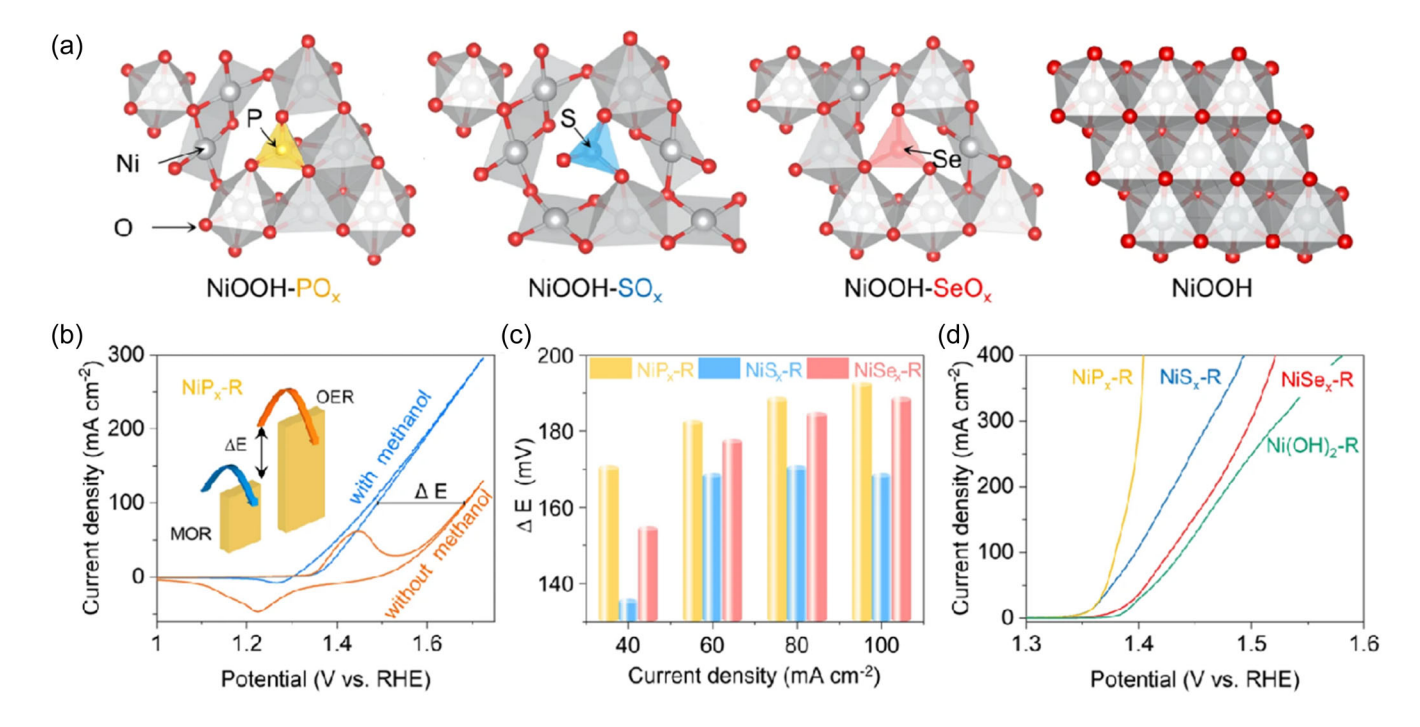


FIGURE 5 (a) Optimized structural models of oxyanions-doped NiOOH and pure NiOOH; (b) CV curves of NiP_x-R in 1 M KOH with/ without 0.5 M MeOH (scan rate: 5 mV s⁻¹); (c) The potential difference between MOR and OER at different current densities. (d) MOR polarization curves of NiT_x-R and Ni(OH)₂-R as the control sample. Reproduced with permission: Copyright 2022, Nature. [57]

Daniel Mandler and the team used iron-substituted lanthanum cobaltite to electrocatalytically oxidize methanol to formic acid. They optimized the MOR catalytic activity and selectivity by adjusting the Fe/Co ratio in the oxide. This adjustment influenced the performance of the catalyst due to the differing affinities of Fe and Co for the reactants CH_3OH and OH^- , respectively. The balance between these affinities in $LaCo_{0.5}Fe_{0.5}O_3$ was favorable, resulting in the highest formate yield. This work demonstrates the importance of precise catalyst design in enhancing the selectivity of methanol oxidation to valuable products.

Guo et al. applied Ni-based medium-entropy alloy aerogels (MEAAs) in the electrocatalytic oxidation of methanol to formic acid. The synthesized Ni $_{50}$ Co $_{15}$ Fe $_{30}$ Cu $_{5}$ MEAAs exhibited a high mass activity of $1.62\,\mathrm{A\,mg^{-1}}$ and a specific activity of $132.24\,\mathrm{mA\,cm^{-2}}$ for MOR, which was much higher than their low-entropy counterparts. The methanol oxidation-assisted MEAAs-based water electrolyzer can achieve a low cell voltage of $1.476\,\mathrm{V}$ at $10\,\mathrm{mA}$ cm $^{-2}$ for value-added formate and $\mathrm{H_2}$ production at the anode and cathode, $173\,\mathrm{mV}$ lower than conventional alkaline water electrolyzers.

Luo and colleagues introduced a new technology for electrodepositing flower-like NiCo₂S₄ nanosheets onto carbon cloth (CC@NiCo₂S₄).^[60] They developed a method to enable energy-efficient H₂ production from water/methanol co-electrolysis at high current densities by constructing array structures and adjusting surface magnetism. By optimizing the electrochemical in-situ growth surface and finely tuning the magnetic properties of CC@NiCo₂S₄ nanosheet arrays, they achieved universal exposure of the (0 1–1) surface, which resulted in high catalytic activity for methanol electrooxidation and long-term stability at high current densities. This innovative approach offers a promising solution for high H₂ production via co-electrolysis of water and methanol.

Qu et al. successfully constructed ultrathin and smaller NiFe-LDH on the surface of SnO2 nanosheets loaded with NF through layer-by-layer assembly. [61] It demonstrated excellent electrocatalytic activity in electrolyte solutions containing 0.5 M methanol and 1 M KOH. Remarkably, only 1.396 V was required to achieve a current density of 10 mA cm⁻², indicating exceptional OER activity. The outstanding OER performance of the catalyst is attributed to the contribution of the semiconductor SnO2 electron transport layer. The three-dimensional structured SnO₂ nanosheets play a crucial role in controlling the growth of ultrathin nickel-iron, and the graded interface between SnO2 and NiFe-LDH influences the electron arrangement around the iron and nickel active centers at the interface. This results in a slight increase in the valence state of iron and an increase in Ni³⁺ content. Moreover, the SnO₂ semiconductor, serving as an electron transport layer, helps capture electrons generated during the oxidation reaction, facilitating the faster transfer of electrons from the NiFe-LDH active center to the Ni substrate and ultimately enhancing the activity of NiFe-LDH.

Xu et al. reported Cu_3N nanosheets with typical antiperovskite structures as electrocatalysts for selective conversion of methanol to formate. The as-prepared antiperovskite nitride Cu_3N sample exhibits a Faradaic efficiency of more than 90% for methanol versus formate over a wide potential range. In addition, high-resolution transmission electron microscopy, XAS and in-situ Raman spectroscopy results indicate that the core-shell structure formed by generating surface Cu (II) species triggers the electrocatalytic MOR activity. During the electrocatalytic process, the original Cu_3N core promotes electron transport inside the catalyst.

Peng and their team employed an ultra-fast solution consumption strategy to synthesize a highly dispersed FeNi oxide heterojunction (Fe₂O₃/NiO) anchored on nickel foam (Figure 6a), creating an efficient catalyst. [63] In the electrooxidation of methanol, this catalyst demonstrated remarkable performance, achieving a high absolute current density (1.654 V at 500 mA cm⁻², Figure 6b-d) with a high Faradaic efficiency (>98%). In-situ infrared spectroscopy and theoretical calculations shed light on the mechanisms behind this exceptional performance. The Fe₂O₃/NiO heterostructure was found to regulate the electronic state of NiO through strong electronic interactions, creating unique synergistic active sites that facilitate the efficient conversion of methanol to formate while inhibiting further oxidation (Figure 6e,f). Additionally, the interfacial confinement effect played a role in stabilizing the metastable nickel active sites, ensuring the structural stability of the catalyst during reversible redox cycles. This resulted in a stable and dynamically enhanced catalytic process for methanol electrooxidation.

Shahrokhian et al. synthesized a petal-like structure of mixed NiCo/NiO-CoO/nanoporous carbon composite (NiCo/NiO-CoO/NPCC) for methanol oxidation through a straightforward method. The unique ultrathin porous petal-like structure with free pores and enlarged specific surface area provides rapid ion/electron transfer, resulting in faster kinetics, lower overpotential, and higher electrocatalytic reactivity. In addition to its interesting structural features, the excellent electrical conductivity of the carbon framework, the rational composition of the two components and the synergistic effect of cobalt, nickel and their oxides provide favorable catalytic activity for methanol electrooxidation.

Fu and colleagues developed a catalyst for methanol electrooxidation by designing an ultrathin nanosheet coated with Ni-Co layered double hydroxide (LDH) on a cobalt

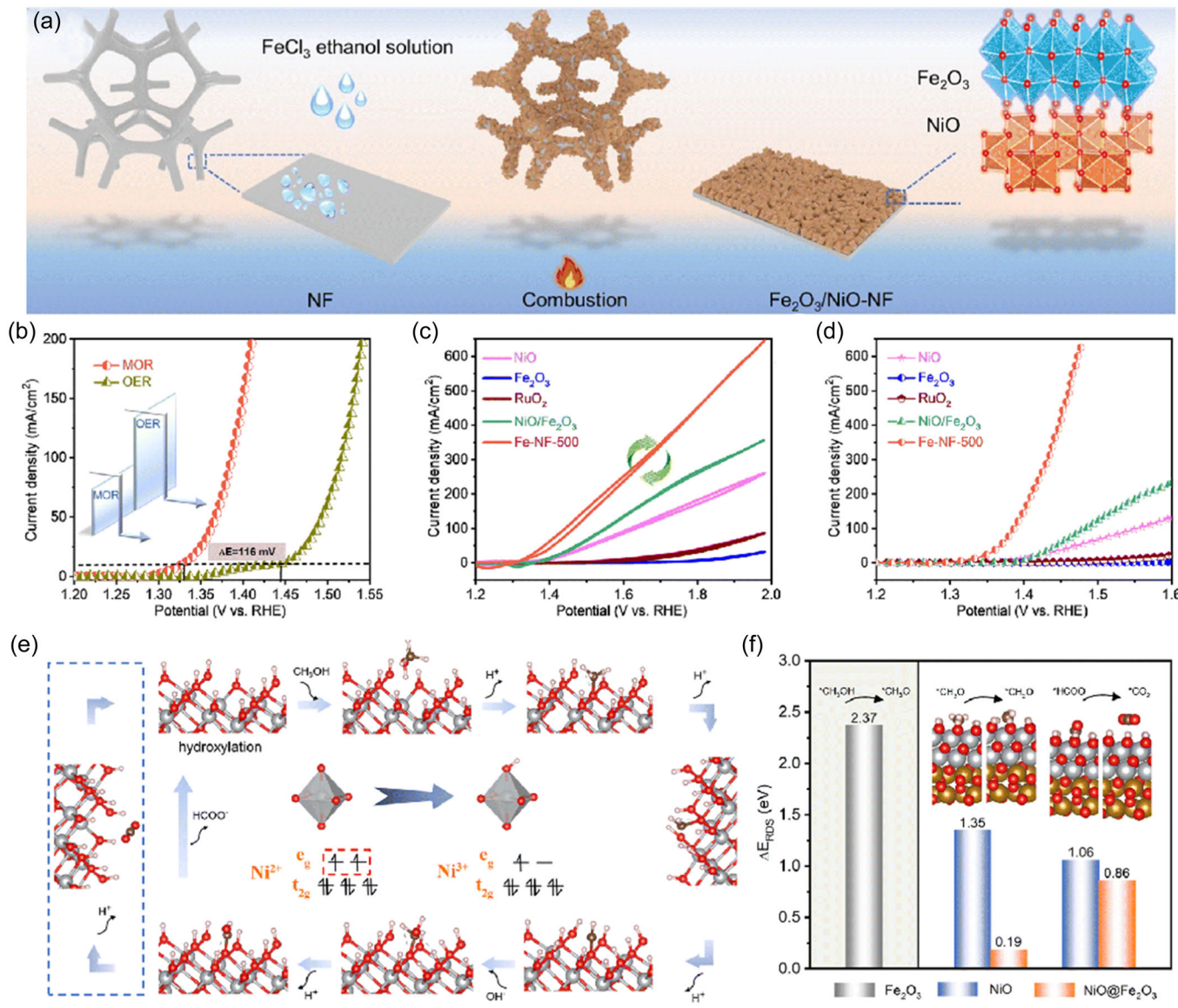


FIGURE 6 (a) Schematic illustration of the preparation process of Fe₂O₃/NiO; (b) Polarization curves of Fe-NF-500 in 1.0 M KOH with/without 1.0 M MeOH. (c) Cyclic voltammograms; (d) Polarization curves of NiO, Fe₂O₃, RuO₂, NiO/Fe₂O₃ mixture, and Fe-NF-500. (e) Schematic of the MOR mechanism for Fe-NF-500. (f) The pivotal potential gaps of RDS (ΔERDS) during the MOR process for the NiO, Fe₂O₃, and Fe₂O₃/NiO. Reproduced with permission: Copyright 2023, RSC. [63]

phosphide nanosheet array. [65] This innovative catalyst, CoxP@NiCo-LDH/nickel foam (NF), capitalizes on the fast charge transfer facilitated by the phosphide nanoarray and leverages the synergistic effects present in the nanosheet structure with heterogeneous interfaces. As a result, this catalyst exhibits exceptional electrocatalytic performance for the electrooxidation of methanol.

3.1.2 **EOR**

Ethanol, a readily available and affordable alcohol, possesses an oxidation potential of 0.084 V (Table 1). Employing nonnoble metal catalysts for ethanol oxidation can reduce the voltage requirements in mixed water electrolysis for hydrogen production. [66] Furthermore, this process yields valuable acetate products at the anode. The EOR is a fourelectron reaction, necessitating efficient and highly active catalysts. Researchers can enhance the electrocatalytic performance of nonprecious metal EOR catalysts through various methods, such as heteroatom doping, defect engineering, and optimizing conductivity. This opens avenues for more energy-efficient hydrogen production and the simultaneous generation of valuable products.

Zheng and colleagues developed a Cu-doped nickel oxyhydroxide catalyst to enhance the efficiency of the EOR. The incorporation of Cu into the catalyst not only increases its specific surface area but also elevates the valence state of Ni. As a result, the catalyst demonstrates remarkable EOR catalytic activity, requiring only $1.72\,V$ to achieve a current density of $227\,mA\,cm^{-2}$. [67]

Sun and colleagues employed metal-organic framework precursors in a one-pot hydrothermal approach to synthesize $Co(OH)_2@Ni(OH)_2$ heterostructures. This catalyst demonstrates excellent catalytic activity for the EOR with an onset potential of 1.30 V and exceptional stability, sustaining over 100 h at 50 mA cm⁻². During the catalytic reaction, ethanol is converted to acetate through a four-electron oxidation process with a remarkable Faradaic efficiency of 97.9%. The superior performance of the catalyst can be attributed to the double hydroxide heterostructure, further enhanced through electrochemical activation. In-situ Raman spectroscopy and DFT calculations have identified Ni (NiOOH) as the pivotal active site for EOR.

Zhuang et al. synthesized defective Ni₃S₂ nanowires (NWs), which exhibit remarkable activity for the electrochemical oxidation of ethanol to acetate. ^[69] These Ni₃S₂-NWs are formed through a directional attachment mechanism, introducing a wealth of defects during their growth process. The electrooxidation of ethanol using the synthesized Ni₃S₂-NWs achieves a low onset potential of 1.31 V and impressive activity of 8716 mA mg_{Ni}⁻¹ at 1.5 V. Notably, the selectivity for acetate reaches approximately 99%. The heightened activity of Ni₃S₂-NWs can be attributed to the facilitated oxidation of Ni (II) to the

catalytically active Ni (III) species, a process promoted by the sulfur component and abundant defects.

Zhai and collaborators assert that, apart from the thermodynamic properties influenced by the electronic structure of the catalyst, the dynamics of molecular and ion movement in the electrolyte significantly impact catalyst efficiency (Figure 7a).[70] Ethanol molecules, due to their relatively large size and viscosity, necessitate spacious channels for molecular and ion transportation through the catalyst. They propose porous CoNi hydroxide nanosheets as exemplary catalysts that synergistically regulate the dynamics of both molecular and electronic structures. Molecular dynamics simulations directly illustrate the capacity of these nanosheets to function as "dams," facilitating the accumulation of ethanol molecules and their enhanced penetration through the nanopores. Furthermore, the presence of heteroatoms alters the charge transfer behavior, which, in turn, modifies local charge density to promote molecular chemisorption. As anticipated, these perforated nanosheets exhibit a low potential (1.39 V) and high Faradaic efficiency in converting ethanol to acetic acid (Figure 7b-d).

By implementing a straightforward fluorination strategy, Cai and colleagues have concurrently achieved both high current and high efficiency in EOR on a NiFe-LDH catalyst. [42] Introducing F into NiFe-LDH reduces the activation energy for the dehydrogenation reaction, consequently enhancing the deprotonation process

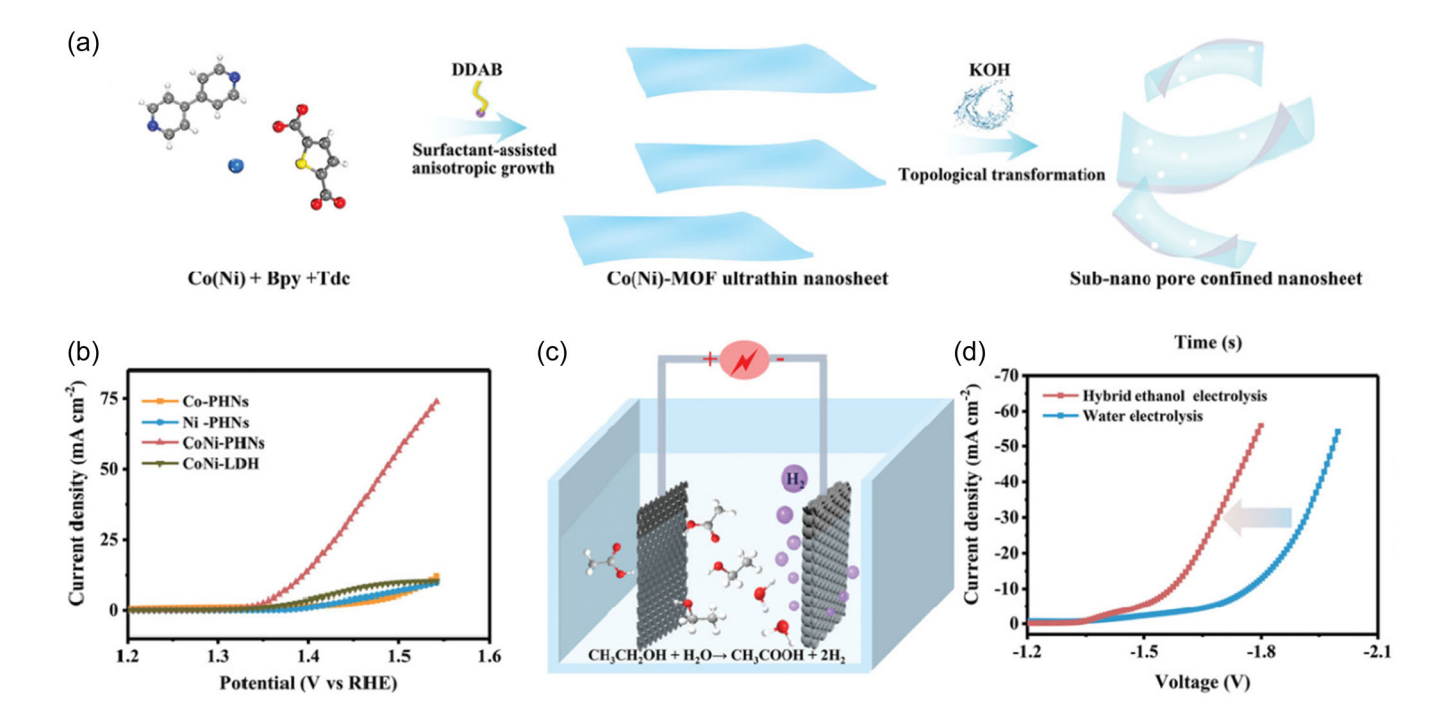


FIGURE 7 (a) Schematic illustration of the synthesis of the CoNi-PHNs; (b) The normalized polarization curves of various catalysts for EOR at a scan rate of 5 mV s⁻¹; (c) The schematic shows the homemade ethanol electrolyzer using the CoNi-PHNs as the anode and CoS_2 -MoS₂ as the cathode; (d) Current-potential curves for CoS_2 -MoS₂//CoNi-PHNs in a two-electrode system in 1.0 M KOH with/without 1.0 M ethanol. Reproduced with permission: Copyright 2019, Wiley. [70]

within NiFe-LDH. This leads to a lowered onset potential for EOR. Additionally, F weakens the adsorption of OH and the electro-oxidation products of organic small molecules, such as ethanol and methanol, on the catalyst at higher potentials, thereby achieving a higher oxidation current density in EOR. This catalyst exhibits low potentials of 1.386 V at 10 mA cm⁻² and 1.423 V at 100 mA cm⁻², lower than those required to attain the same current density in the OER. Moreover, it maintains a Faradaic efficiency higher than 95% over a broad current density range from 10 to 250 mA cm⁻², indicating remarkable selectivity.

Wang and collaborators employed the highly electronegative fluorine element to finely tune the binding energy between the Fe sites (FeOOH) and reactants (OH or $C_2H_5O^-$), resulting in more optimized adsorption characteristics. This adjustment simultaneously enhances the positive charge density on Fe sites, promoting the OER and EOR. Consequently, this integration of OER and efficient anodic behavior for ethanol oxidation reduces the electrolysis voltage of 1.43 V to achieve a current density of 10 mA cm⁻² for hydrogen production.

3.1.3 | Brief summary

Low-grade fatty alcohols, characterized by a single hydroxyl functional group, exhibit a relatively clear reaction mechanism. Their good water solubility is advantageous for achieving high current in industrial condition. Additionally, these alcohols, owing to their widespread availability, affordability, and potential for generating high-value oxidation products, are extensively studied in AORs. Among the nonprecious metals investigated for their catalytic activity in the oxidation of lower fatty alcohols, Ni, Co, Fe, and Cu have been reported, with Ni-based materials demonstrating particularly high activity. Strategies commonly employed in the design of OER catalysts, such as heteroatom doping, electron cloud regulation, heterojunction design, defect introduction, and conductivity optimization, can also be applied to synthesize catalysts for the oxidation of low-grade fatty alcohols. The primary design focus for these catalysts is directed toward the unique reaction characteristics that distinguish them from OER.

3.2 | Catalysts for polyhydric alcohol

3.2.1 | Ethylene glycol oxidation reaction (EGOR)

Ethylene glycol, a basic polyol, plays a pivotal role as a monomer in producing a widely used plastic known as polyethylene terephthalate (PET). PET is among the most prevalent disposable household plastics, with millions of tons produced annually.^[72] The extensive use of PET and increasing environmental concerns have accentuated the need for efficient and sustainable recycling methods. [73] In response to these demands, electrochemical strategies for PET degradation and recycling have come to the forefront, centering on the electrocatalytic oxidation of ethylene glycol. This process enables the efficient conversion of ethylene glycol into formate, a valuable compound, using nonprecious metal catalysts. Importantly, this electrochemical process can be coupled with the HER to produce hydrogen and formate.^[74] In recent years, there has been a surge in research reports detailing the design and development of EGOR catalysts. These developments hold great promise for advancing the field of electrochemical PET recycling and contribute to a more sustainable approach for dealing with PET waste.[75]

Zhao and colleagues made a pioneering contribution by introducing and documenting an electrochemical upcycling approach that utilizes copper-based nanowire catalysts for the electrocatalytic oxidation of PET hydrolysis products. [76] This innovative electrocatalyst effectively facilitates the conversion of ethylene glycol molecules derived from PET waste into formate, demonstrating a remarkable selectivity for this conversion process. Furthermore, it exhibits a lower onset potential for EG oxidation than water oxidation. Both experimental evidence and DFT calculations support the notion that the ethylene glycol oxidation pathway on CuO selectively cleaves C-C bonds, generating formic acid. This approach presents a significant advancement in the field of PET recycling.

Duan and collaborators designed an electrocatalyst based on nickel-modified cobalt phosphide (CoNi_{0.25}P).^[77] This catalyst could reach a current density of 500 mA cm⁻² at 1.8 V in an MEA reactor while maintaining a Faradaic efficiency and selectivity of over 80% for formate production (Figure 8a–d). Indepth characterization of the CoNi_{0.25}P catalyst unveiled an in-situ transformation into a low-crystalline metal-oxygen (hydroxide) state during the oxidation of EG, which likely contributes to its impressive performance. This research provides a sustainable approach to repurposing waste PET into valuable products.

Zhu and team innovatively developed atomic nickel-modified CoP electrocatalysts using ordered macroporous ZIF-67 single crystals as a foundation. The catalyst boasts a meticulously structured macroporous superstructure complemented by abundant inherent mesopores. These unique structural features contribute significantly to its outstanding catalytic activity. When

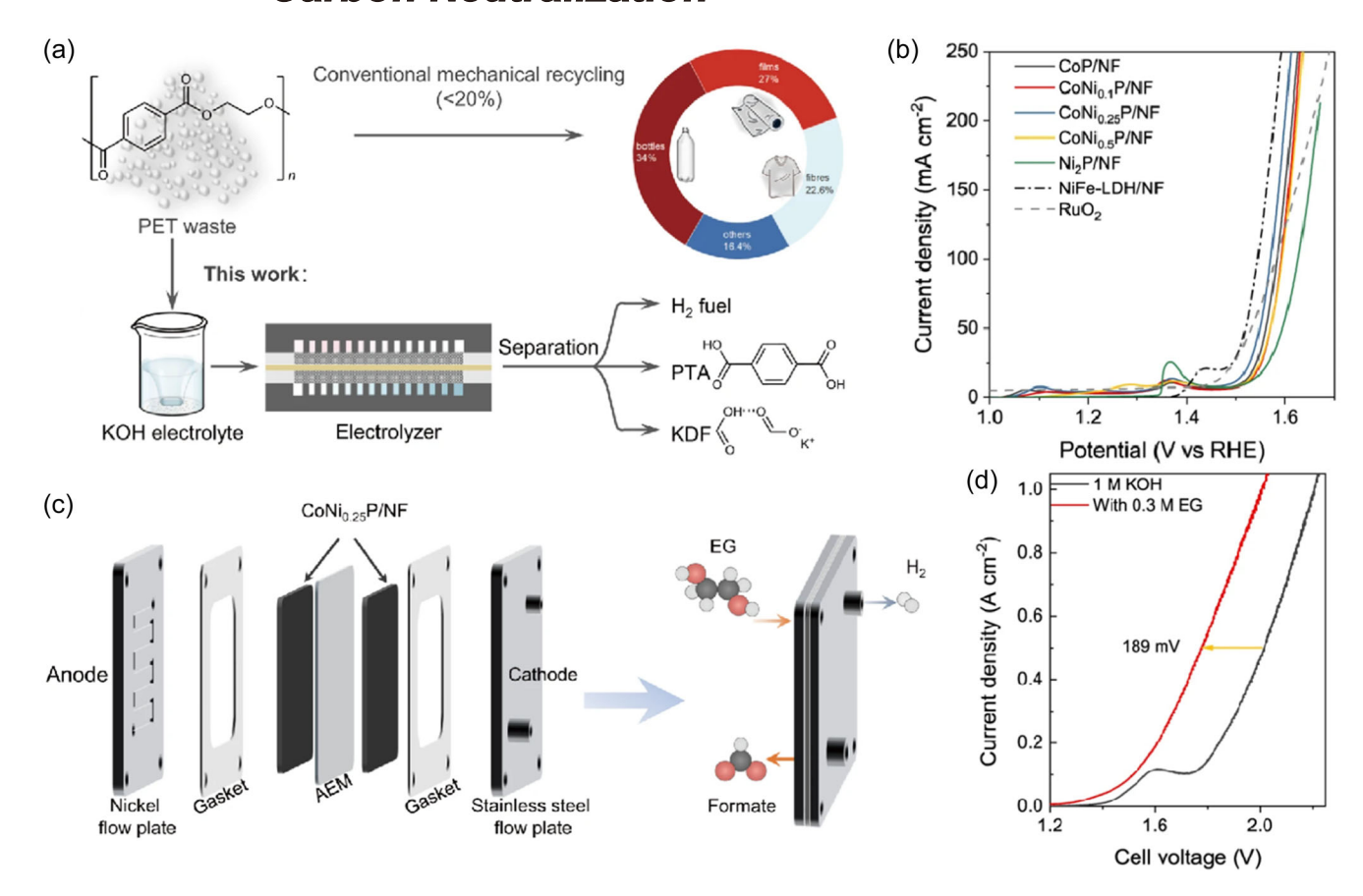


FIGURE 8 (a) Electrocatalytic PET upcycling to commodity chemicals and H₂ fuel; (b) LSV curves (85% iR corrected) for EGOR; (c) The MEA setup for paired HER//EGOR; (d) Polarization curves for water splitting and EG electrolysis in the MEA flow reactor at a scan rate of 10 mV s⁻¹. Reproduced with permission: Copyright 2023, Nature.^[77]

subject to further electrochemical restructuring, this catalyst, in a composite electrolyte consisting of an alkaline electrolyte and PET plastic hydrolyzate, demonstrates exceptional performance, achieving a high Faradaic efficiency of up to 96% for the EGOR. Remarkably, this bifunctional electrocatalyst, both in hydrogen evolution and producing commodity chemicals, facilitates an innovative, energy-efficient approach to electrolysis.

Chen and their research team presented their work on the electrocatalytic reforming of ethylene glycol (EG) derived from PET, employing a Ni(OH)₂/Ni foam catalyst. Significantly, this catalyst maintains over 90% Faradaic efficiency and selectivity, even at industrially significant current densities exceeding 500 mA cm⁻² at 1.60 V. In-situ electrochemical Raman spectroscopy revealed that NiOOH rapidly forms at relatively low potentials in the presence of EG and plays a pivotal role in the oxidation of EG derived from PET. Compared with the OER, the substantial production of NiOOH results in a substantial electrical potential difference of 430 mV at 100 mA cm⁻², consequently enhancing the Faradaic efficiency of EGOR. This research marks a significant advancement in the recycling of PET waste.

Ma and colleagues introduced an electrocatalytic integration strategy to efficiently harness PET plastic and CO₂ to produce formic acid at both electrodes simultaneously. The NiCo₂O₄ electrocatalyst demonstrated an impressive Faradaic efficiency of 90% for formic acid production, indicating outstanding selectivity for the oxidation of PET hydrolyzate. By pairing the PET hydrolyzate oxidation reaction with the CO₂ reduction reaction, the assembled electrolyzer showcased a low cell voltage of 1.55 V to facilitate the two integrated half-reactions. Moreover, at a cell voltage of 1.90 V, formic acid achieved an exceptional Faradaic efficiency of 155%. This innovative approach promotes PET recycling and produces a surplus of high-quality formic acid production.

Ni and their team engineered a high-performance nickel sulfide catalyst for electro-recycling plastic waste using a co-doping strategy involving cobalt and chloride. [81] The combined dopants shifted the d-band center and promoted in-situ structural reconstruction by leveraging an interconnected ultrathin nanosheet structure. This Co and Cl co-doped Ni₃S₂ catalyst, denoted as Co, Cl-NiS, outperformed its single-doped and undoped

counterparts in electrocatalytic EGOR. The self-evolving sulfide@oxyhydroxide heterostructure enabled the efficient conversion of ethylene glycol to formate, achieving high Faradaic efficiency (>92%) and selectivity (>91%) even at elevated current densities (>400 mA cm⁻²). Notably, beyond formate production, the bifunctional Co, Cl-NiS-assisted PET hydrolyzate electrolyzer exhibited a remarkable hydrogen production rate of 50.26 mmol h⁻¹ at 1.7 V in a 2 M KOH electrolyte. This breakthrough demonstrates a highly efficient and selective approach to recycling plastic waste while producing valuable products.

3.2.2 | Glycerol oxidation reaction (GOR)

Glycerol, a cost-effective byproduct of the biodiesel production industry, possesses a significantly lower theoretically required oxidation potential (0.003 V, as indicated in Table 1) than OER (1.23 V). [82] Using nonnoble metal catalysts, glycerol can be efficiently oxidized, producing formic acid, a higher-value product. [82] Consequently, GOR has emerged as a promising alternative to coupled HER electrolysis for hydrogen generation. [83] In recent years, research in the field of GOR has gained momentum, with researchers achieving high-performance GOR catalysts through various strategies, including single-atom doping, oxygen vacancy construction, and anion intercalation. [84]

Li and colleagues introduced a ligand intercalation strategy in which they intercalated sodium dodecyl sulfate (SDS) into the interlayer of a Co(OH)₂ catalyst, forming Co(OH)₂-SDS.^[85] Compared with pure Co(OH)₂, Co(OH)₂-SDS exhibits a significantly enhanced current density for glycerol electrooxidation. At a potential of 1.42 V, the corresponding glycerol conversion rate and H₂ production rate reached 0.35 mmol cm⁻² h⁻¹ and 9.1 mL cm⁻² h⁻¹, respectively. These values are 2.2 times and 1.9 times higher than those achieved with Co(OH)₂. With a glycerol conversion rate of 95.1% (resulting in a glycerol oxidation FE of 83.3%), the formate yield reaches 86.6%, and the selectivity is 95.3%.

Chen and their team have discovered that protons and oxygen within the crystal lattice play active roles in catalytic reactions and are crucial in determining reactivity. Using the electrooxidation of glycerol as a model reaction, they systematically elucidated the impact of protons and oxygen anions' (de)intercalation process on the fundamental reaction steps. By employing a combination of DFT calculations and advanced spectroscopic techniques, they observed that introducing Co into nickel hydroxide promotes the deintercalation of protons and oxygen anions from the catalyst's surface. During the

electrooxidation of glycerol, the resulting oxygen vacancies in NiCo hydroxide increase the filling of the d-band on the Co sites, facilitating charge transfer from the surface to the broken molecules during the second C-C bond cleavage process. As a result, NiCo hydroxide exhibits enhanced electrooxidation activity for glycerol, achieving a current density of 100 mA cm⁻² and a formate selectivity of 94.3% at a voltage of 1.35 V.

Duan et al. reported a single-atom bismuth (Bi) doping strategy to enhance the activity and selectivity of Co_3O_4 for electrocatalytic GOR (Figure 9a). Experimental characterization and theoretical calculations show that single-atom bismuth replaces cobalt at the octahedral position $(\text{Co}_{\text{Oh}}^{3+})$ of Co_3O_4 , promoting the generation of reactive hydroxyl species (OH*) at the adjacent tetrahedral Co site $(\text{Co}_{\text{Td}}^{2+})$. Mechanistic studies show that OH* accelerates the oxidation of hydroxyl groups and the cleavage carbon-carbon (C–C) bonds. Therefore, GOR activity (400 mA cm⁻² at 1.446 V, Figure 9b,c) and high Faradaic efficiency of formate (97.05 \pm 2.55%) were achieved.

Yu et al. conducted a study in which they selected CoO and Co_3O_4 as representative cobalt oxide catalysts. These catalysts were grown on carbon fiber paper (CFP) electrodes to explore the interplay between electronic structure and catalytic activity, particularly in glycerol, diols, and monohydric alcohol oxidation. [88] In-situ electrochemical tests revealed that, compared with the Co₃O₄/CFP electrode, the CoO/CFP electrode exhibited lower interface resistance, higher charge transfer efficiency, and a faster oxidation rate, resulting in significantly enhanced catalytic activity for alcohol oxidation. Notably, regarding glycerol oxidation, the CoO/CFP electrode only required 1.32 V to achieve a current density of 10 mA cm⁻², representing a substantial potential reduction of 120 mV compared with the Co₃O₄/CFP electrode. Furthermore, the CoO/CFP electrode demonstrated the capacity to generate value-added products, including formate, acetate, and glycolate, via the oxidation of biomass alcohols, all achieved with high selectivity and reduced energy consumption. Theoretical calculations further underscored the crucial role of octahedral-coordinated Co-O sites in the adsorption, activation, and oxidation of C3-C1 alcohols. This study contributes valuable insights into designing efficient transition metal oxide catalysts for alcohol oxidation, emphasizing the significance of filling octahedral sites within the crystal structure.

Wen and their research team conducted experimental work to prepare a novel self-supporting electrode composed of a high-entropy alloy (HEA).^[36] This electrode featured uniform HEA nanoparticles grown on carbon cloth, and systematic electrochemical investigations revealed its

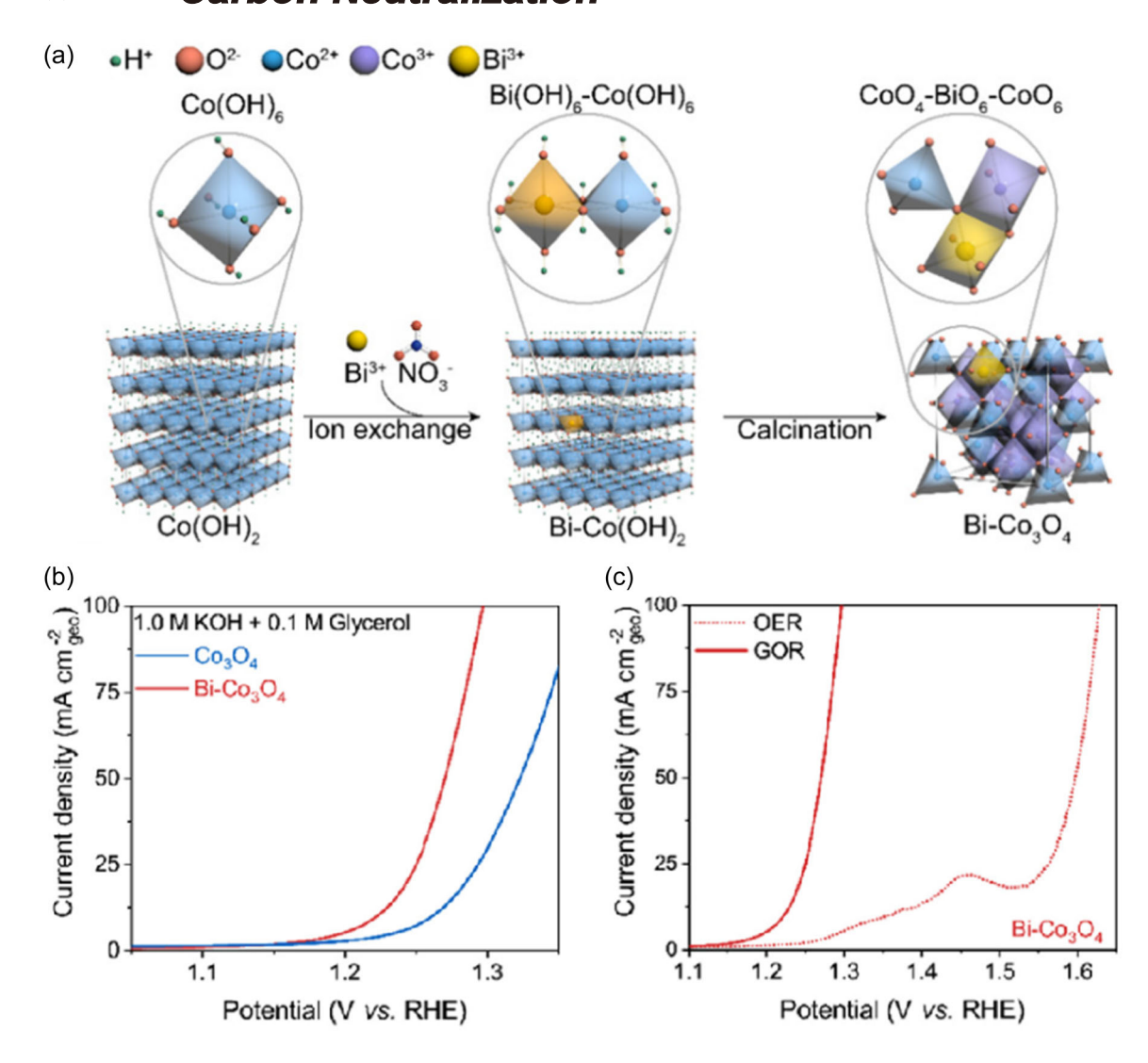


FIGURE 9 (a) Schematic illustration of the synthesis strategy for single-atom Bi-doped Co_3O_4 catalyst; (b) 90% iR-corrected LSV curves of Co_3O_4 and Bi- Co_3O_4 in 1.0 M KOH with 0.1 M glycerol at a scan rate of 5 mV s⁻¹; (c) Catalytic activity comparison of Bi- Co_3O_4 in OER and GOR. Reproduced with permission: Copyright 2022, ACS.^[87]

impressive performance as an electrocatalyst for GOR. The HEA-CoNiCuMnMo electrode exhibited low overpotential and a remarkable selectivity for formate product formation. Detailed scrutiny of the surface atomic configuration of HEA-CoNiCuMnMo was facilitated by a customdeveloped Monte Carlo simulation based on machine learning. This analysis identified the catalytic active center at the Mo site, coordinated by Mn, Mo, and Ni. By coupling the alkaline GOR with an acidic HER using HEA-CoNiCuMnMo as the anode and commercial RhIr/Ti as the cathode, the researchers successfully achieved an electrolysis current density of 10 mA cm⁻² with an impressively low voltage of 0.55 V. Furthermore, this electrolysis system demonstrated long-term stability during continuous operation at 50 mA cm⁻² for 12 days. The Faradaic efficiency of H₂ production at the cathode exceeded 99%, while the Faradaic efficiency for formate production at the anode reached 92%. This research showcases a promising approach to efficiently harness glycerol oxidation and underscores the importance of these findings for future applications in renewable energy production.

Zhang et al. designed and synthesized a transition metal nitride heterojunction catalyst (dual-phase Ni_3N/Co_3N heterostructure nanowire) grown in situ on nickel foam. The rich electronic regulation of the heterojunction interface enables it to exhibit excellent dual catalytic activity in catalyzing mixed glycerol oxidation-assisted hydrogen production.

Gong and collaborators conducted research involving the incorporation of chelated phenanthroline into the bulk phase of nickel hydroxide. By modifying functional groups, they successfully adjusted the material's electronic properties, resulting in tunable selectivity for formate (with levels of up to 92.7%) and oxalate (reaching levels of up to 45.3%). [82]

27693335, 2024. 2. Downloaded from https://onlinelibtrary.wiley.com/doi/10.1002/cm2.116 by James Cook University. Wiley Online Library on [26/11/2025]. See the Terms and Conditions (https://onlinelibtrary.wiley.com/ems-and-conditions) on Wiley Online Library for rules of use; OA articles are governed by the applicable Creative Commons Licensed

Importantly, this tunability exhibited a nearly linear relationship with the Hammet parameter, an essential descriptor in organic chemistry. Subsequent investigations involved an in-depth analysis of intermediates and the application of various spectroscopic techniques. These studies unveiled a delicate balance in the probability of further C-C cleavage or oxidation reactions of the intermediates. This equilibrium was achieved by modulating the valence band of the key glycolaldehyde intermediate, a pivotal factor in influencing the selectivity of the oxidation process. This work offers valuable insights into the precise control of reaction pathways in catalytic processes, which is significant for developing more efficient and selective chemical transformations.

Guo et al. prepared a self-supporting high-entropy selenide (HESe) electrode by in-situ growth on copper foam (CF). [90] Electrochemical test results show that HESe exhibits high electrocatalytic activity for GOR, requiring only 1.20 V to reach a current density of 10 mA cm⁻². HESe maintains high selectivity for formate products over a wide potential range (1.27-1.57 V), and the GOR reaction mechanism was verified by in situ IR. The lattice changes of HESe were studied through XRD, HR-TEM and in-situ Raman, and the lattice distortion effect between metals in HESe was verified.

3.2.3 Brief summary

Polyhydric alcohols have two or more hydroxyl groups, resulting in a more complex reaction mechanism and more oxidation products. The involvement of C-C bond cleavage further complicates the exploration of their catalytic oxidation mechanisms. The design of nonprecious metal catalysts for polyhydric alcohol oxidation often draws inspiration from strategies employed in the design of OER and low-grade fatty alcohol oxidation catalysts. Researchers typically employ trial-and-error strategies to identify high-performance catalytic materials. Presently, reported polyhydric alcohol oxidation catalysts primarily target the production of formats, with limited reports on other oxidation products. Consequently, a promising direction for the catalytic synthesis of polyhydric alcohol oxidation involves designing catalysts with high selectivity and activity for different oxidation products.

3.3 Catalysts for aromatic alcohol

3.3.1 | Benzyl alcohol oxidation reaction (BAOR)

Benzyl alcohol, the most basic aromatic alcohol, is a precursor for synthesizing valuable chemicals such as benzaldehyde and benzoic acid. [91] It features a notably lower electrochemical catalytic oxidation potential compared with OER. [92] Furthermore, owing to its distinctive benzene ring structure, which results in limited solubility, there is potential for selective catalysis of its oxidation into benzaldehyde using nonprecious metal materials.

Wang and colleagues successfully achieved the selective electrooxidation of alcohols to aldehydes using NiO by fine-tuning the local microenvironment to separate aldehydes from the reaction system.^[93] The crux of this remarkable selectivity lies in inhibiting aldehyde hydration, which is attributed to reduced alkalinity and elevated cation and substrate concentrations. This strategic approach allows for the complete and exclusive extraction of aldehydes from the gas/ electrolyte interface during alcohol electrooxidation, and its applicability readily extends to other selective oxidation reactions.

Research on the electrooxidation of benzyl alcohol mostly uses benzoic acid as the target product and synthesizes high-performance BAOR catalysts through a series of designs. An and colleagues engineered nickel nanoparticles (Ni-NPs) with various sizes supported on nitrogen-doped carbon (NC).[94] They achieved this by precisely controlling the pyrolysis temperature, yielding Ni@NC-500 (8.3 nm), Ni@NC-280 (1.9 nm), and Ni@NC-200 (1.0 nm). When applied in the electrooxidation of benzyl alcohol (BA), these nanocatalysts exhibited benzoic acid yields of 99%, 82%, and 55%, respectively. Experimental examinations and theoretical simulations were conducted on Ni@NC-280, Ni@NC-200, and Ni@NC-500. The results revealed that disparities in the adsorption strength of Ni-NPs to reactive molecules account for their distinct properties.

Wang and his research team developed a selfsupporting, hierarchical, porous nitrogen-doped carbon (NC)@CuCo₂N_x/carbon fiber (CF) composite. They applied it to the selective electrooxidation of benzyl alcohol in an alkaline solution. [95] This catalyst exhibited both remarkable conversion rates and selectivity. The outstanding electrocatalytic performance is primarily ascribed to the hierarchical structure, which promotes the exposure of numerous catalytically active sites and enhances mass transport. The DFT calculations have revealed that the synergistic interplay between CoN and CuN is pivotal in fine-tuning the adsorption energy of key species.

Qiu's research team synthesized an amorphous nanosheet (A-Ni-Co-H/NF) comprising Ni and Co hydroxides supported on Ni foam.[37] This catalyst features a substantial active area and low charge transfer resistance and is employed to catalyze the electrocatalytic oxidation of benzyl alcohol (Figure 10a). A-Ni-Co-H/NF

(a) Traditional water electrolysis:

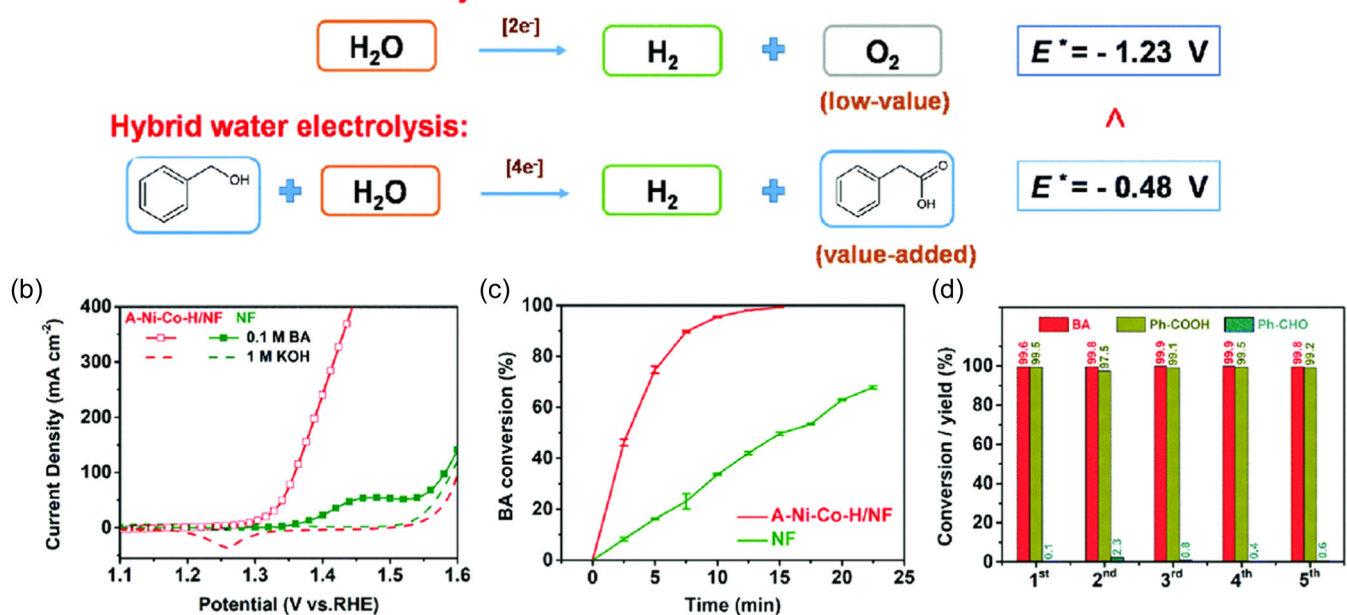


FIGURE 10 (a) The related reactions of traditional water electrolysis and hybrid water electrolysis; (b) LSV curves of A-Ni-Co-H/NF and NF in 1 M KOH with and without 0.1 M BA (scan rate: 10 mV s⁻¹); (c) Conversion variation of BA with the time of the amperometric tests at 1.5 V versus RHE in the electrolyte with 1 M KOH and 0.1 M BA using A-NiCo-H/NF and NF as the electrocatalysts; (d) the conversion of BA and the yield of its oxidation products. Reproduced with permission: Copyright 2020, RSC.^[37]

enables the achievement of industrial-scale current densities exceeding $400\,\mathrm{mA\,cm^{-2}}$ without the need for OER, demonstrating ultrafast reaction kinetics (Figure 10b). The yield of Ph-COOH approaches 100% (Figure 10c,d). In-situ Raman spectroscopy provided evidence of the reversible structural evolution and recovery of the A-Ni-Co-H/NF catalyst during the electrochemical oxidation of benzyl alcohol. The transformed species, particularly Co-containing nickel oxyhydroxide (Co-NiOOH), was identified as the authentic active component. Ma et al. found that compared with $\mathrm{Co_3O_4}$ nanoparticles, $\mathrm{Co_3O_4}$ nanoneedle arrays have better e-BAOR activity. [87] The electrooxidation of benzyl alcohol can achieve a conversion rate of >99% and a selectivity of 92% to benzoic acid.

Wang and their research team demonstrated the use of cobalt/iron (oxide) heterostructures with interface engineering to finely adjust surface structural properties, resulting in enhancements for both the OER and BAOR processes. [96] The engineering of the interface induced local crystallinity and the formation of defective oxygen sites, enabling the material to achieve an OER of 50 mA cm⁻² at an overpotential of 329 mV, with continuous operation for 20 h without significant degradation. Moreover, the heterostructure also demonstrated improved performance in BAOR, further advancing water splitting to generate 10 mA cm⁻² at a voltage of only 1.42 V. Theoretical calculations elucidated that defect

sites dominated by the interface facilitate the adsorption and dissociation of intermediates during the electrocatalytic process.

Lei and collaborators synthesized a Co₃O₄-based catalyst through an innovative one-step hydrothermal process, which was subsequently confirmed to be rich in oxygen vacancies (VO) and cobalt vacancies (V_{Co}).^[97] This electrocatalyst for the oxidation of benzyl alcohol (BA) consists of vacancy-rich Co₃O₄ on nickel foam (NF) with an optimized electronic structure. It demonstrates an ultrahigh conversion rate (99%) and selectivity (99%) toward benzoic acid (BAc), showcasing excellent recyclability and ranking among the top-performing cobalt-based catalysts. Analytical techniques, such as XPS and XANES, in conjunction with DFT calculations, reveal that the conspicuous electron delocalization induced by vacancies not only reduces the adsorption energy of BA but also enhances the intrinsic activity of the catalytic Co sites, thus accelerating the reaction kinetics. Moreover, the band gap is reduced, leading to improved conductivity.

Sun and the research team employed a straightforward and environmentally friendly template-free electrodeposition method to create 3D hierarchical porous nickel-based electrocatalysts for an integrated electrolysis process. Notably, this approach required a voltage of approximately 220 mV below the water-splitting voltage to achieve a current density of 50 mA cm⁻². This

electrocatalyst exhibits robust stability, high Faradaic efficiency, an absence of reactive oxygen species (ROS) formation, and the generation of valuable products both at the cathode (H₂) and the anode (alcohol oxidation products). Importantly, it was observed that the oxidation of various alcohols on hp-Ni exhibits similar onset potentials, primarily determined by the desired oxidation potential of hp-Ni itself. These onset potentials remain largely independent of the distinct intrinsic thermodynamics of the oxidation reactions for these alcohols.

Qu and colleagues presented a theoretical explanation in which they pointed out that β -NiOOH dominated by OH* exhibits inherently low reactivity toward the α -C-H bonds in alcohols, thereby limiting their activation and dissociation. Conversely, β -NiOOH, primarily composed of O*, displays higher reactivity, leading to a more potent activation and dissociation of α -C-H bonds. Considering the operational characteristics, the research team demonstrated that phytase could establish a β -NiOOH surface primarily consisting of O* on the nickel foam during operation. This surface modification significantly increased the electrooxidation activity of benzyl alcohol, enhancing it by an impressive factor of 10.2. [99]

Duan and the research team systematically upgraded lignin derivatives into carboxylates using a catalyst based on Mn-doped cobalt oxyhydroxide (MnCoOOH).[100] They efficiently cleaved various lignin-derived substrates containing C(OH)-C or C(O)-C units, forming corresponding carboxylates with excellent yields ranging from 80% to 99% and impressive operational stability for 200 h. In their comprehensive studies, the researchers unveiled the oxidation mechanism, in which the base present in the electrolyte converts secondary alcohols and their derivative ketones into reactive nucleophiles. These nucleophiles are subsequently oxidized by electrophilic oxygen species on MnCoOOH within a water-based environment. As a proof of concept, this method was applied to upgrade lignin derivatives featuring C(OH)-C or C(O)-C motifs, resulting in the conversion of a ligninderived mixture into benzoate ester with a remarkable yield of 91.5% and the conversion of KA oil into adipate ester with a yield of 64.2%.

Yu and their research team achieved the direct growth of 2D Ni-based nanoarrays (CC@NiO/Ni $_3$ S $_2$) on carbon cloth (CC) substrates. [101] CC@NiO/Ni $_3$ S $_2$ comprises ultrathin nanosheets measuring approximately 3.4 nm and features abundant NiO/Ni $_3$ S $_2$ heterointerfaces. This unique structure offers several advantages as it exposes more active sites and enhances the diffusion of mass and charge. Furthermore, it fosters unique interfacial interactions that facilitate charge redistribution, activating the formation of critical reaction intermediates. As a result, CC@NiO/Ni $_3$ S $_2$ exhibits a low

overpotential of only 91 mV to achieve a current density of 10 mA cm^{-2} and demonstrates high catalytic stability for the HER. When employed as a catalyst for the electrooxidation of benzyl alcohol, rather than water oxidation, $CC@NiO/Ni_3S_2$ displays excellent catalytic activity and a high selectivity of over 98% in the production of benzoic acid. Consequently, utilizing $CC@NiO/Ni_3S_2$ as cathode and anode electrocatalysts for HER and Ph-CH₂OH oxidation, respectively, leads to a stable generation of hydrogen fuel and the production of valuable Ph-COOH. Importantly, by substituting Ph-CH₂OH oxidation for water oxidation, the H₂ generation rate increases by 2.6 times at a cell voltage of 1.609 V, and this modification results in a 10.0% reduction in electrical energy consumption at a current density of 50 mA cm^{-2} .

Lu's team employed a straightforward electrodeposition method to create a porous electrode of transition metal hydroxide (M(OH)2, where M=Ni or Co) nanosheets on a Ni foam substrate. [102] They then assessed the catalytic performance of this porous electrode in the electrooxidation of benzyl alcohol in a NaOH aqueous solution. The results indicated that, for the electrooxidation of benzyl alcohol, the Ni(OH)2 nanosheet/Ni foam electrode displayed a higher current density than the Co (OH)₂ nanosheet/Ni-foam electrode. Notably, the Ni (OH)₂ nanosheet electrode achieved a remarkable feat: it required an extremely low potential of approximately 1.33 V to reach a current density of 100 mA cm⁻². Furthermore, the durability tests demonstrated that the Ni(OH)₂ nanosheet electrode exhibited excellent stability when subjected to the electrooxidation of benzyl alcohol. Moreover, by utilizing noble metal-free catalysts, this electrode enabled the eco-friendly synthesis of benzoic acid through the electrooxidation of benzyl alcohol in a two-electrode configuration while concurrently generating hydrogen. When benzyl alcohol was completely oxidized, the optimal selectivity for benzoic acid and the Faradaic efficiency of benzyl alcohol electrooxidation reached 96% and 95%, respectively.

3.3.2 | Brief summary

Aromatic alcohols have poor water solubility due to the presence of benzene rings, which do not support achieving high current oxidation. The efficient electrocatalytic synthesis of their oxidation products has emerged as a crucial objective in the field of aromatic alcohol oxidation. Current reports predominantly focus on carboxylic acid products as the primary oxidation outcome. However, aldehyde products, despite their higher added value, exhibit poor stability. Consequently, the pursuit of efficient aromatic alcohol oxidation

necessitates considerations not only for catalyst design but also for the composition of the electrolyte. In terms of catalyst design, the achievement of efficient aldehyde product production primarily involves adjusting the adsorption of intermediate species through the regulation of the electron cloud structure. Simultaneously, in the realm of electrolytes, it has been observed that the salt-out effect proves beneficial for generating aldehyde products.

4 | AOR CATALYST APPLICATION

The initial aim of AOR research was to substitute the OER reaction in alkaline electrolysis for hydrogen production, aiming to curtail electricity consumption. [103] Since most of the AOR products are dissolved in the electrolyte, high-purity hydrogen can be produced with only a simple electrolysis device (without a specific ion exchange membrane), further reducing the cost of hydrogen production. The alcohol water electrolysis system is an extension of the alkaline water electrolysis system. Due to the continuous consumption of substrates by AOR, a flow cell is requisite to attain high current and sustained hydrogen production over the electrolysis period. Simultaneously, to accommodate different reduction reactions such as CO₂RR, NO₃RR, and other diverse electrolysis environments, the introduction of an ion exchange membrane is necessary to segregate the anode and cathode electrolytes.

4.1 | Coupled with HER

The primary objective in developing efficient AOR catalysts is to leverage AOR as a substitute for OER, coupled with HER, to reduce the voltage required for electrolytic hydrogen production. [104] Utilizing nonprecious metal-based materials to catalyze AOR reactions can generally decrease the voltage needed for the electrolysis hydrogen production cell by 100–500 mV. [105] This process also yields valuable carboxylate products at the anode, with higher economic value than oxygen. Notably, the AOR product remains within the electrolyte, eliminating safety concerns associated with subsequent gas separation or the risk of hydrogen and oxygen mixing. Over recent years, researchers have made significant strides in developing a series of highly active and selective AOR catalysts. These catalysts have been successfully integrated into alcohol-water electrolysis systems, with their economic viability diligently assessed. [106]

Zhao and colleagues employed CoNi-PHNs as anodic EOR catalysts to facilitate coupled HER (utilizing CoS₂-MoS₂ as the HER catalyst) in the context of hybrid water electrolysis.^[70] It was observed that the voltage required for hybrid water electrolysis was lower than that needed for overall water decomposition across various current densities. Moreover, at a potential of 1.75 V, the Faraday efficiency for hydrogen reached 90.5%, and notably, no oxygen was generated during the electrocatalytic process. Additionally, the dual-electrode configuration exhibited an impressive Faraday efficiency of 94.1% for acetate production.

Duan et al. constructed a zero-gap MEA flow reactor, employing CoNi_{0.25}P/NF catalysts as cathode and anode. ^[77] Overall, water electrolysis and EG electrolysis displayed nearly identical polarization curves. Test results indicate that when achieving the same current density in the presence of EG in the analyte, the battery voltage decreases by approximately 189 mV, enhancing cathode energy efficiency. The MEA reactor demonstrates significantly higher current density (500 mA cm⁻²) at a low battery voltage (<1.8 V) while maintaining a Faraday efficiency of over 80%.

Zhu et al. employed the previously reported OMS-Ni₁-CoP as the electrode catalyst in an assembled dual-electrode electrolytic cell. [78] In the HERI|EGOR electrolysis system, OMS-Ni₁-CoP/OMS-Ni₁-CoP achieved a current density of 10 mA cm⁻² at 1.52 V, which is 160 mV lower than the current density in the HER||OER system, highlighting the energy-saving advantage of utilizing EGOR over OER. OMS-Ni₁-CoP/OMS-Ni₁

Wang et al. presented the utilization of NC@CuCo $_2N_x$ /CF as an electrocatalyst for efficient HER, OER, and BAOR reactions. They employed NC@CuCo $_2N_x$ /CF as the electrocatalyst for both electrodes, establishing a dual-electrode electrolytic cell for the selective electrochemical oxidation of hydrogen production and benzyl alcohol. This configuration demonstrated high conversion rates and selectivity.

In a methanol-mixed water electrolysis system, Guo et al. utilized $\rm Ni_{50}Co_{15}Fe_{30}Cu_5$ medium entropy alloy aerogels (MEAAs). ^[59] In comparison to pure water electrolysis, their designed methanol oxidation-assisted water electrolysis cell exhibited a lower cell voltage of 1.476 V in a 1.0 M KOH solution containing 1.0 M methanol while still achieving a current density of $10\,\rm mA\,cm^{-2}$. This voltage was notably lower than that

of traditional water electrolysis cells, which typically operate at 1.649 V. Peng et al. employed the previously reported Fe-NF-500 as the anode and MoNi₄ as the cathode to create a dual-electrode system for alcoholwater electrolysis. The Fe-NF-500||MoNi₄ electrode combination achieved current densities of 10 mA cm⁻² for the anode and 500 mA cm⁻² for the cathode at potentials of 1.381 V and 1.654 V, respectively. These potentials were significantly lower than those required for OER to achieve similar current densities.

Ma et al. developed vertical NiO thin sheets and NiMoNH nanopillars, which improved the reaction kinetics of anodic GOR and cathodic HER, respectively. [107] At the same time, to eliminate the explosion risk of mixed $\rm H_2/O_2$, cheap organic membranes are used to replace the expensive anion exchange membranes in the electrolytic cell. GOR-assisted hydrogen production (HER||GOR) only requires a battery voltage of 1.54 V at a current density of 100 mA cm⁻². The operating voltage of the electrolytic cell is significantly reduced by 280 mV and exhibits excellent long-term stability.

Finally, as a brief summary of this section, we would like to emphasize that the important purpose of developing AOR is to reduce the energy consumption of electrolytic hydrogen production by coupling HER to reduce cell voltage. Numerous studies have demonstrated that replacing the OER with AOR can effectively lower the voltage of the electrolysis hydrogen production cell by 100-500 mV. Additionally, AOR can yield products with higher added value than O₂ at the anode. Implementing an actual AOR coupled HER system not only places higher demands on the catalyst but also necessitates specific requirements for cell types and the flow rate of electrolyte components. Catalysts exhibiting excellent performance are predominantly Nibased catalysts supported on foam nickel, while the flow cell demonstrates a lower voltage for hydrogen production compared with the H-type cell.

4.2 | Coupled with other reactions (CO₂RR, NO₃RR, etc.)

After clarifying the role of AOR in reducing cell voltage, [108] researchers embarked on coupling AOR with other cathodic reduction reactions, [109] simultaneously generating high-value products at both the cathode and anode. [31]

4.2.1 | Coupled with CO_2RR or CORR

Ma et al. utilized the reported $NiCo_2O_4/CFP$ catalyst to oxidize PET hydrolysis products and SnO_2/CC as the

anode for CO₂ reduction to generate formic acid. These materials were assembled into a two-electrode electrolytic cell. [80] The electrolytic cell with 0.1 M PET hydrolysate exhibited a significantly low cell voltage of 1.55 V and a higher catalytic current. A catalytic current of 20 mA cm⁻² was achieved at a voltage of 1.9 V, which is approximately 180 mV lower than traditional CO₂RR without the assistance of PET hydrolysis product oxidation. The coupled electrolytic cell also demonstrated a remarkable 155% increase in Faradaic efficiency for formic acid production at 1.9 V. This enhancement is attributed to the simultaneous production of formic acid at both the anode and cathode. The replacement of OER with PET hydrolysis product oxidation reduces energy consumption, increases the value of PET plastic waste, and enhances the utilization value of anode production and the Faradaic efficiency of the target product.

Wen et al. assembled a flow electrolysis cell based on the reported NiSAs/FN-CNSs and $CoSe_2/CC$ catalysts. [110] In this system, NiSAs/FN-CNSs acted as the cathode for electrocatalytic CO_2 reduction to produce CO, while $CoSe_2/CC$ functioned as the anode for electrocatalytic glycerol oxidation to generate formate. The cathode and anode electrolytes were continuously circulated in a solution containing $2.0\,\mathrm{M}$ KHCO $_3$ and $2.0\,\mathrm{M}$ glycerol within a $2.0\,\mathrm{M}$ KOH environment. Remarkably, the electrolysis achieved a current density of $100\,\mathrm{mA\,cm^{-2}}$ at a voltage of only $1.97\,\mathrm{V}$, resulting in a high Faraday efficiency of 90% for both cathode CO and anode formate production. This innovative use of glycerol oxidation in place of OER contributed to a significant 20% reduction in electricity consumption

Lu et al. designed a two-electrode electrolytic cell to produce formate simultaneously at the cathode and anode of $\rm CO_2RR$ and $\rm MOR$. The electrolytic cell uses $\rm CuSn$ -4 as the anode and cathode, with $\rm CO_2$ -saturated 0.5 M KHCO₃ and 1 M KOH + 1 M CH₃OH as the cathode and anode electrolytes. Specifically, the $\rm CO_2RR$ -MOR system provides a current density of $\rm 100~mA~cm^{-2}$ at a cell voltage of 3.23 V, 610 mV lower than the $\rm CO_2RR$ -OER system (3.84 V). In the $\rm CO_2RR$ -MOR system, the faradaic efficiency for formate production reached 73.1% at the cathode and 81.7% at the anode.

Jiao introduced an innovative internal coupling purification strategy to significantly enhance the concentration and purity of acetic acid produced via CO electroreduction. This approach employs an anion exchange membrane with excellent alkaline stability and high ethanol permeability in conjunction with a selective ethanol partial oxidation anode to regulate the flow of CO reduction products. Demonstrated results indicated that the CO electrolyzer operated consistently for 120 h at a current density of 200 mA cm⁻² and maintained a

is) on Wiley Online Library for rules of use; OA articles are governed by the applicable Creative Commons License

voltage of less than 2.3 V, thereby continuously generating 1.9 M acetic acid with an impressive purity of 97.7%. Through fine-tuning reaction conditions, the purity of the acetic acid stream was further elevated to 99%, accompanied by a concentration of 7.6 M. Ultimately, a detailed technical and economic analysis underscored the importance of a highly concentrated liquid product stream in reducing energy consumption during product separation.

4.2.2 | Coupled with NRR or NO₃RR

Shi et al. established a two-electrode electrolytic cell for NRR and MOR (Figure 11a-b), where Bi/Bi₂O₂CO₃-NS was used as the cathode in a 0.1 M Na₂SO₄ electrolyte, and NiCo-DH-Bi-NS was used as the anode in a 1 M KOH electrolyte containing 3 M MeOH (Figure 11c). Compared with the situation without the addition of methanol, the required cell voltage at 10 mA cm⁻² was reduced by 251 mV (Figure 11d-f), which means that the energy consumption of ammonia production is significantly reduced compared with a typical nitrogen water co-electrolysis system. The electrolytic cell showed a

maximum NH_3 production of 2.787 mg h^{-1} cm⁻² at 2.2 V. Furthermore, even after 30 h of operation at 2.2 V, there was no significant decline in current density, which underscores the exceptional stability of the system.

Wang et al. prepared a nonprecious metal NiCu-OH nanocomposite precatalyst composed of crystalline Cu₂(OH)₃(NO₃) and amorphous Ni(OH)₂.^[114] Under operating conditions, the catalyst can be reconstructed into highly active and stable cathode NO₃RR and anode GOR electrocatalysts. Under anodic GOR conditions, NiCu-OH-derived bimetallic oxides (NiCuO) transform into active NiOOH species that combine with CuO rich in Cu vacancies.

Shao's team introduced an efficient bifunctional electrocatalyst comprising cobalt phosphide loaded on a carbon nanosheet array (CNs@CoP). This catalyst was employed in a coupled system involving the electrocatalytic nitrate reduction reaction (NITRR, NO₃RR) and GOR. [115] Compared with the NITRR||OER and HER||GOR systems, the NITRR||GOR coupled system demonstrated superior selectivity and yield for nitrate reduction and glycerol oxidation. Specifically, the NITRR||GOR coupling system achieved a FE of 96.4% and a 15.2 mg h $^{-1}$ cm $^{-2}$ ammonia yield, along with a 93.5% FE and a 65.6 mg h $^{-1}$ cm $^{-2}$ formic acid yield

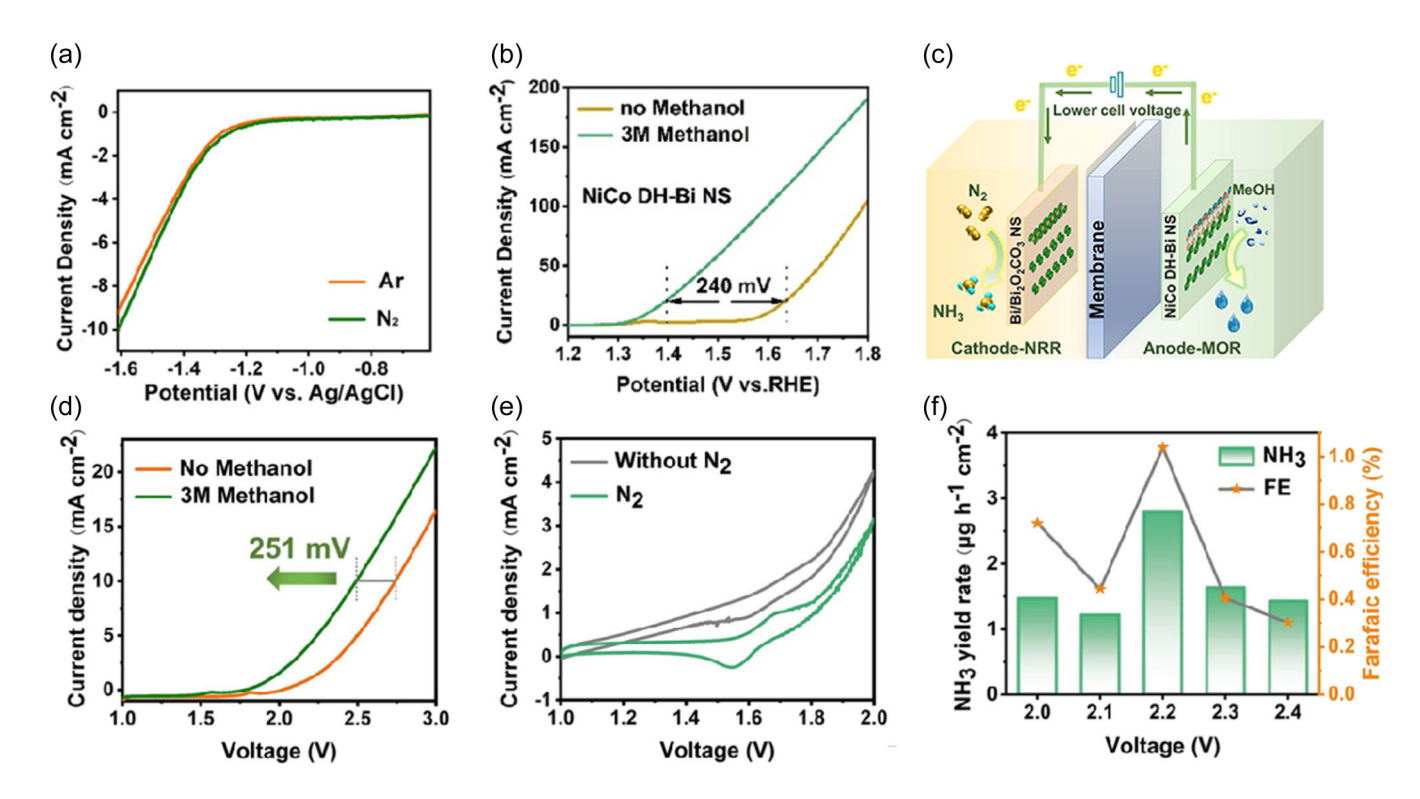


FIGURE 11 (a) LSV curves for the Bi/Bi₂O₂CO₃ NS in N₂ and Ar saturated 0.1 M Na₂SO₄ solution; (b) LSV curves for the NiCo DH-Bi NS in 1 M KOH with/without 3 M MeOH; (c) Schematic illustration for the electrode catalyst syntheses and nitrogen-methanol coelectrolysis system; (d) LSV curves of the electrolyzer with and without the addition of 3 M MeOH; (e) Cyclic voltammetry plots of the electrolyzer in 1 M KOH with 3 M MeOH; (f) NH₃ yields and FEs of the electrolyzer at different applied potentials. Reproduced with permission: Copyright 2022, Cell Press. [113]

27693335, 2024. 2. Downloaded from https://onlinelibtrary.wiley.com/doi/10.1002/cm2.116 by James Cook University. Wiley Online Library on [26/11/2025]. See the Terms and Conditions (https://onlinelibtrary.wiley.com/ems-and-conditions) on Wiley Online Library for rules of use; OA articles are governed by the applicable Creative Commons Licensed

at a high current density of 300 mA cm⁻². Notably, the formic acid generated at the anode in this electrolysis system can be further upgraded into high-value potassium formate.

4.2.3 | Other applications

Based on the innovative idea of replacing OER with EOR, Sun et al. synthesized a heterogeneous Co(OH)₂@Ni (OH)₂ catalyst using a one-pot hydrothermal method as the cathode. They designed a mixed water electrolysis and zinc ethanol air battery.^[68] The advantage of this design is that the total potential of water decomposition is reduced by 200 mV, the charging voltage of the battery is reduced by 300 mV, and the direct utilization of biomass energy is achieved.

4.2.4 | Brief summary

In addition to being used to couple HER for efficient hydrogen production, AOR is also used to couple CO₂RR, CORR, NRR, and NO₃RR. It is worth noting that the basis for introducing AOR reaction instead of OER reaction into other electrolysis systems is that AOR significantly reduces the voltage of the electrolysis cell, and can also produce high value-added chemicals at the anode and cathode. Given the different electrolysis environments at the anode and cathode, the integration of AOR with other reaction systems necessitates more sophisticated electrolysis devices. This includes the utilization of ion exchange membranes to effectively separate different products (Table 2).

5 | SUMMARIES AND OUTLOOK

This review provides a comprehensive review of recent advancements in nonprecious metal catalysts designed for the electrooxidation of alcohols, encompassing both mechanistic investigations and the development of high-performance catalysts. The AOR offers a theoretically more ideal oxidation potential than the OER, resulting in a lower cell voltage for hydrogen production coupled with HER. This leads to a reduction in energy consumption during electrolytic hydrogen production, mitigates safety concerns associated with hydrogen-oxygen mixing and avoids the use of diaphragms. Additionally, the AOR is the foundational step for producing various high-value products. Electrocatalytic alcohol oxidation represents an efficient and environmentally friendly process, enabling

the rapid generation of high-value products. Given these advantages, AOR has attracted significant attention from researchers. However, due to its multielectron reaction step, AOR exhibits sluggish kinetics, necessitating the development of efficient catalysts to expedite the reaction rate.

Consequently, numerous nonprecious metal catalysts have been devised for AOR catalysis. Furthermore, proposed AOR catalytic mechanisms for nonprecious metal catalysts include the two-step nucleophile oxidation mechanism, lattice oxygen mechanism, and traditional adsorption reaction mechanism. Many high-performance AOR catalysts are also employed coupled with cathode reactions like HER, CO₂RR, CORR, NO₃RR, and NRR, yielding notable improvements in energy efficiency (Figure 12).

While significant efforts have been made in fabricating various materials that exhibit exceptional performance in AOR, the advancement of electrocatalysts continues to depend heavily on performance-driven trial-and-error approaches. To enhance the preparation of catalytic materials that are both highly active and selective for AOR, several pivotal issues and challenges still require resolution:

- 1. To identify the active sites, the prevailing perspective suggests that the hydroxyl oxides formed following the restructuring of nonprecious metals are active species. Further research is required to elucidate their influence on the pre-catalyst reconstruction and subsequent catalytic processes. Moreover, the effects of materials like foam nickel carbon cloth, typically viewed as conductive substrates, on the catalytic process warrant further investigation.
- 2. There is a need for a more in-depth investigation into the AOR mechanism. The AOR reaction displays distinct reaction characteristics based on the applied potential. While researchers have employed various in-situ physical and electrochemical testing methods to monitor species changes during the AOR process and have put forth corresponding catalytic mechanisms, these existing mechanisms can only account for the reaction characteristics of AOR under specific conditions (like a particular potential range or current range) and do not provide a comprehensive or precise description of the entire AOR process.
- 3. Using theoretical calculations to aid in exploring reaction mechanisms is promising. The catalytic properties of AOR display a significant association with the electrolyte environment, including factors such as acidity and alkalinity. However, traditional DFT calculations have not fully accounted for the

TABLE 2 Comparison of recently reported nonprecious metal-based electrocatalysts for AORs in different electrolysis systems.

Electrolytic system and electrocatalyst	Cell voltage	Anolyte	FE of oxidation product	Cell type	Product	Reference
HER: $Ni_{50}Co_{15}Fe_{30}Cu_5 MOR: Ni_{50}Co_{15}Fe_{30}Cu_5$	$1.476 \mathrm{V}$ at $10 \mathrm{mA cm^{-2}}$	1 M KOH + 1 M MeOH	ı	Nonmembrane cell	H ₂ & Formate	[59]
HER: CC@NiCo ₂ S ₄ MOR: CC@NiCo ₂ S ₄	$1.32/1.81 \mathrm{V}$ at $10/100 \mathrm{mA cm^{-2}}$	1 M KOH + 1 M MeOH	~100%	Nonmembrane cell	H_2 & Formate	[09]
HER: MoNi4 MOR: Fe-NF-500	$1.381/1.654 \mathrm{V}$ at $10/500 \mathrm{mA cm^{-2}}$	1 M KOH + 1 M MeOH	I	Nonmembrane cell	$ m H_2$ & Formate	[63]
HER: Co _x P@NiCo-LDH/NF MOR: Co _x P@NiCo-LDH/NF	$1.43\mathrm{V}$ at $10\mathrm{mAcm^{-2}}$	1 M KOH + 0.5 M MeOH	~100%	H-type cell	H_2 & Formate	[65]
HER: OMS-Ni ₁ -CoP EGOR: OMS-Ni ₁ -CoP	$1.52\mathrm{V}$ at $10\mathrm{mAcm}^{-2}$	1 M KOH + 0.5 M EG	93.2%	Nonmembrane cell	H_2 & Formate	[78]
HER: NIMoNHIIGOR: NiO	1.54V at 100 mA cm ⁻²	1 M KOH + 0.1 M glycerol	1	AEM flow cell	H_2 & Formate	[107]
HER: hp-NillBAO: hp-Ni	$1.50/1.66 \text{ V}$ at $10/1.00 \text{ mA cm}^{-2}$	1 M KOH + 10 mM BA	%26~	AEM cell	H_2 & benzoic acid formation	[86]
CO ₂ RR: SnO ₂ /CC EGOR: NiCo ₂ O ₄ /CFP	$1.90 \mathrm{V}$ at $20 \mathrm{mA cm^{-2}}$	0.1 M PET hydrolysate	85%	I	Formate	[80]
CO ₂ RR: NiSAs/FN-CNSsIIGOR: CoSe ₂ /CC	$1.97 \mathrm{V}$ at $100 \mathrm{mA cm}^{-2}$	2 M KOH + 2 M glycerol	%06	Flow cell	CO& Formate	[110]
CO ₂ RR: CuSn-4 MOR: CuSn-4	$3.23 \mathrm{V}$ at $100 \mathrm{mA cm}^{-2}$	1 M KOH + 1 M MeOH	81.7%	PEM cell	Formate	[111]
CO ₂ RR: BiOBrl GOR: Ni _x B		1 M KOH + 1 M glycerol	~71%	AEM flow cell	Formate	[116]
NRR: Bi/Bi ₂ O ₂ CO ₃ NSIIMOR: NiCo DH-Bi NS	\sim 2.5 V at 10 mA cm ⁻²	1 M KOH + 3 M MeOH	ı	Flow cell	NH ₃ & Formate	[113]
NO ₃ RR: R-NiCu-OHIIGOR: R-NiCuO	~1.8 V at 300 mA cm ⁻²	1 M KOH + 0.1 M glycerol	I	AEM flow cell	NH3& Formate	[114]

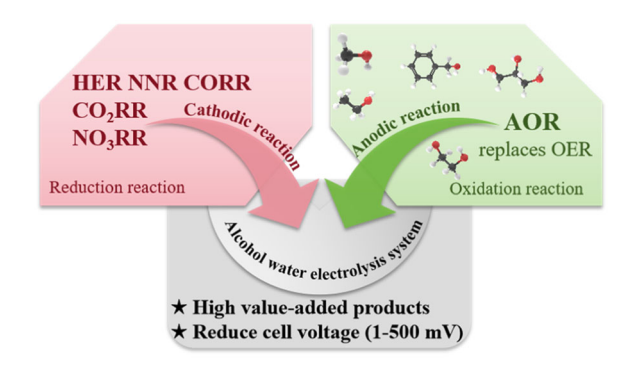


FIGURE 12 Various alcohol water electrolysis systems and advantages.

presence of reactants and the influence of the solvent environment. Therefore, future work should be devoted to theoretical calculation research more consistent with actual reaction conditions.

- 4. The design of AOR catalysts is currently rooted in the established standards for OER catalysts, with a shortage of tailored catalyst designs specifically for AOR. In reality, numerous reported catalysts display specific activity for AOR, and a fundamental comprehension of the distinctions between AOR and OER is pivotal for the precise regulation and manipulation of desired product selectivity.
- 5. Most reported AOR catalysts exhibit a maximum oxidation current density below 500 mA cm⁻², which challenges meeting the criteria for industrial-grade hydrogen production through coupled HER. This issue is intertwined with the intrinsic properties of alcohol molecules, such as slow mass transfer rates and the catalyst itself. Careful considerations must encompass electrolysis equipment and catalyst design to attain high-current AOR-coupled hydrogen production.
- 6. There are currently few reports on the separation and purification of AOR catalytic products, so the cost caused by product separation is not included in the cost of the alcohol-water electrolysis system. To promote the practical application of alcohol-water electrolysis systems, it is imperative to advance a more encompassing economic and technical analysis, one that duly incorporates considerations for product separation.

The challenges mentioned above represent significant hurdles in advancing the field of electrocatalytic AOR, including its role in enabling efficient H_2 (NH₃, etc.) production and alcohol refining and electrolysis systems. In addition to the conventional trial-and-error approach employed for synthesizing high-performance AOR catalysts, artificial intelligence and machine

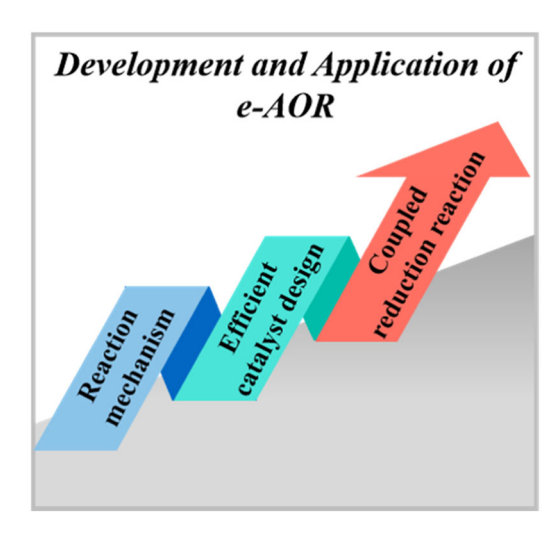


FIGURE 13 Exploring reaction mechanisms and designing efficient catalysts to support the development and application of e-AOR on Precious-Metal-Free catalysts.

learning have accelerated catalyst screening, reduced the cost of efficient catalyst production, and are poised to gain increasing prominence in various electrocatalyst design domains. This review comprehensively outlines AOR's reaction pathways and mechanisms when catalyzed by nonprecious metal materials and the design strategies for high-performance catalysts tailored to various AOR scenarios. We believe this review gives readers a deeper understanding of fundamental principles and offers insights into the rational design of molecular-level electrocatalysts (Figure 13).

AUTHOR CONTRIBUTIONS

Conceptualization: Jiawei Shi and Weiwei Cai. Visualization: Jiawei Shi and Weiwei Cai. Writing—original draft: Jiawei Shi, Jun Ma, Enze Ma, Jing Li, Yang Hu, Liyuan Fan, and Weiwei Cai. Writing—revised version and editing: Jiawei Shi, Liyuan Fan, and Weiwei Cai. Supervision: Weiwei Cai.

ACKNOWLEDGMENTS

We are grateful for financial support from the National Natural Science Foundation of China (22179121), the Knowledge Innovation Program of Wuhan-Basic Research (2022010801010202), and the Research Fund Program of Guangdong Provincial Key Laboratory of Fuel Cell Technology (FC202201).

CONFLICT OF INTEREST STATEMENT

The authors declare no conflict of interest.

REFERENCES

 J. Kang, X. Qiu, Q. Hu, J. Zhong, X. Gao, R. Huang, C. Wan, L.-M. Liu, X. Duan, L. Guo, Nat. Catal. 2021, 4, 1050.

of use; OA articles are governed by the applicable Creative Commons License

WILEY- Carbon Neutralization

- [2] J. Shi, S. Lv, L. Zhang, J. Li, S. Zhou, K. Qu, W. Cai, ACS Appl. Mater. Interfaces 2021, 13, 48962.
- [3] J. Shi, H. Shao, F. Yang, J. Li, L. Fan, W. Cai, Chem. Eng. J. 2022, 445, 136628.
- [4] S. Zhou, Y. Liu, J. Li, Z. Liu, J. Shi, L. Fan, W. Cai, Green Energy. Environ. 2022. In press. https://doi.org/10.1016/j. gee.2022.12.003
- [5] P. Li, Y. Jiang, Y. Hu, Y. Men, Y. Liu, W. Cai, S. Chen, *Nat. Catal.* 2022, 5, 900.
- [6] M. Bajdich, M. García-Mota, A. Vojvodic, J. K. Nørskov, A. T. Bell, J. Am. Chem. Soc. 2013, 135, 13521.
- [7] H. Zhang, P. Li, S. Chen, F. Xie, D. J. Riley, Adv. Funct. Mater. 2021, 31, 2106835.
- [8] J. Li, D. Chu, H. Dong, D. R. Baker, R. Jiang, J. Am. Chem. Soc. 2019, 142, 50.
- [9] B. Zhu, B. Dong, F. Wang, Q. Yang, Y. He, C. Zhang, P. Jin, L. Feng, *Nat. Commun.* 2023, 14, 1686.
- [10] D. Y. Chung, P. P. Lopes, P. Farinazzo Bergamo Dias Martins,
 H. He, T. Kawaguchi, P. Zapol, H. You, D. Tripkovic,
 D. Strmcnik, Y. Zhu, S. Seifert, S. Lee, V. R. Stamenkovic,
 N. M. Markovic, *Nat. Energy* 2020, 5, 222.
- [11] B. J. Kim, E. Fabbri, D. F. Abbott, X. Cheng, A. H. Clark, M. Nachtegaal, M. Borlaf, I. E. Castelli, T. Graule, T. J. Schmidt, J. Am. Chem. Soc. 2019, 141, 5231.
- [12] M. Zhang, Y. Liu, B. Liu, Z. Chen, H. Xu, K. Yan, ACS Catal. 2020, 10, 5179.
- [13] Z. Li, Y. Yan, S. M. Xu, H. Zhou, M. Xu, L. Ma, M. Shao, X. Kong, B. Wang, L. Zheng, H. Duan, *Nat. Commun.* 2022, 13, 147.
- [14] B. Mondal, N. Karjule, C. Singh, R. Shimoni, M. Volokh, I. Hod, M. Shalom, Adv. Energy Mater. 2021, 11, 2101858.
- [15] X. Mu, X. Gu, S. Dai, J. Chen, Y. Cui, Q. Chen, M. Yu, C. Chen, S. Liu, S. Mu, Energy Environ. Sci. 2022, 15, 4048.
- [16] Y. Sun, J. Wang, Y. Qi, W. Li, C. Wang, Adv. Sci. 2022, 9, e2200957.
- [17] S.-K. Geng, Y. Zheng, S.-Q. Li, H. Su, X. Zhao, J. Hu, H.-B. Shu, M. Jaroniec, P. Chen, Q.-H. Liu, S.-Z. Qiao, *Nat. Energy* 2021, 6, 904.
- [18] B. Yang, Y. Yu, J. Qiao, L. Yuan, X. Shen, X. Hu, Appl. Surf. Sci. 2020, 513, 145808.
- J. Li, X. Wang, C. Xing, L. Li, S. Mu, X. Han, R. He, Z. Liang,
 P. Martinez, Y. Yi, Q. Wu, H. Pan, J. Arbiol, C. Cui,
 Y. Zhang, A. Cabot, *Chem. Eng. J.* 2022, 440, 135817.
- [20] D. M. Morales, D. Jambrec, M. A. Kazakova, M. Braun, N. Sikdar, A. Koul, A. C. Brix, S. Seisel, C. Andronescu, W. Schuhmann, ACS Catal. 2022, 12, 982.
- [21] A. Saxena, S. Kapila, J. E. Medvedeva, M. Nath, ACS Appl. Mater. Interfaces 2023, 15, 14433.
- [22] C. Coutanceau, S. Baranton, WIREs Energy Environ. 2016, 5, 388.
- [23] N. Wu, M. Zhai, F. Chen, X. Zhang, R. Guo, T. Hu, M. Ma, Nanoscale 2020, 12, 21687.
- [24] S. Barwe, J. Weidner, S. Cychy, D. M. Morales, S. Dieckhöfer, D. Hiltrop, J. Masa, M. Muhler, W. Schuhmann, *Angew. Chem. Int. Ed.* 2018, 57, 11460.
- [25] M. Yang, Z. Yuan, R. Peng, S. Wang, Y. Zou, Energy Environ. Mater. 2021, 5, 1117.
- [26] N. A. M. Barakat, M. Motlak, Appl. Catal., B 2014, 154-155, 221.

- [27] S. Verma, S. Lu, P. J. A. Kenis, Nat. Energy 2019, 4, 466.
- [28] Y. Song, Z. Li, K. Fan, Z. Ren, W. Xie, Y. Yang, M. Shao, M. Wei, Appl. Catal., B 2021, 299, 120669.
- [29] D. Gupta, A. Kafle, T. C. Nagaiah, Small 2023, 19, e2208272.
- [30] Y. Wu, K.-K. Lu, L.-H. Xu, J. Mater. Chem. A 2023, 11, 17392.
- [31] S. Zhao, T. Wang, Z. Ji, Y. Song, Y. Li, J. Liu, W. Hu, Appl. Catal., B 2023, 320, 122024.
- [32] X. Wei, Y. Li, L. Chen, J. Shi, Angew. Chem. Int. Ed. 2021, 60, 3148.
- [33] Y. L. Zhang, K. Goh, L. Zhao, X. L. Sui, X. F. Gong, J. J. Cai, Q. Y. Zhou, H. D. Zhang, L. Li, F. R. Kong, D. M. Gu, Z. B. Wang, *Nanoscale* 2020, 12, 21534.
- [34] T. Wang, X. Cao, L. Jiao, Angew. Chem. Int. Ed. 2022, 61, e202213328.
- [35] C. Deng, C. Y. Toe, X. Li, J. Tan, H. Yang, Q. Hu, C. He, Adv. Energy Mater. 2022, 12, 2201047.
- [36] L. Fan, Y. Ji, G. Wang, J. Chen, K. Chen, X. Liu, Z. Wen, J. Am. Chem. Soc. 2022, 144, 7224.
- [37] H. Huang, C. Yu, X. Han, H. Huang, Q. Wei, W. Guo, Z. Wang, J. Qiu, Energy Environ. Sci. 2020, 13, 4990.
- [38] B. Zhou, C.-L. Dong, Y.-C. Huang, N. Zhang, Y. Wu, Y. Lu, X. Yue, Z. Xiao, Y. Zou, S. Wang, J. Energy Chem. 2021, 61, 179.
- [39] M. Cai, Y. Zhang, Y. Zhao, Q. Liu, Y. Li, G. Li, J. Mater. Chem. A 2020, 8, 20386.
- [40] W. Chen, C. Xie, Y. Wang, Y. Zou, C.-L. Dong, Y.-C. Huang, Z. Xiao, Z. Wei, S. Du, C. Chen, B. Zhou, J. Ma, S. Wang, *Chem* 2020, 6, 2974.
- [41] J. Shao, Y. Fang, X. Wu, M. I. Abdullah, Y. Tao, Nano Res. 2023. In press. https://doi.org/10.1007/s12274-023-6078-z
- [42] J. Shi, H. He, Y. Guo, F. Ji, J. Li, Y. Zhang, C. Deng, L. Fan, W. Cai, J. Energy Chem. 2023, 85, 76.
- [43] Y. Qi, Y. Zhang, L. Yang, Y. Zhao, Y. Zhu, H. Jiang, C. Li, Nat. Commun. 2022, 13, 4602.
- [44] H. Cheng, B. Dong, Q. Liu, F. Wang, J. Am. Chem. Soc. 2023, 145, 26858.
- [45] P. Chandrasekharan Meenu, P. K. Samanta, T. Yoshida, N. J. English, S. P. Datta, S. A. Singh, S. Dinda, C. Chakraborty, S. Roy, ACS Appl. Energy Mater. 2022, 5, 503.
- [46] F. Meng, Q. Wu, K. Elouarzaki, S. Luo, Y. Sun, C. Dai, S. Xi, Y. Chen, X. Lin, M. Fang, X. Wang, D. Mandler, Z. J. Xu, Sci. Adv. 2023, 9, eadh9487.
- [47] W. Chen, J. Shi, C. Xie, W. Zhou, L. Xu, Y. Li, Y. Wu, B. Wu, Y.-C. Huang, B. Zhou, M. Yang, J. Liu, C.-L. Dong, T. Wang, Y. Zou, S. Wang, *Natl. Sci. Rev.* 2023, 10, nwad099.
- [48] W. Chen, J. Shi, Y. Wu, Y. Jiang, Y. C. Huang, W. Zhou, J. Liu, C. L. Dong, Y. Zou, S. Wang, Angew. Chem. Int. Ed. Engl. 2024, 63, e202316449.
- [49] B. You, X. Liu, N. Jiang, Y. Sun, J. Am. Chem. Soc. 2016, 138, 13639.
- [50] Y. Lu, L. Zhou, S. Wang, Y. Zou, Nano Res. 2022, 16, 1890.
- [51] X. Wang, S. Xi, W. S. V. Lee, P. Huang, P. Cui, L. Zhao, W. Hao, X. Zhao, Z. Wang, H. Wu, H. Wang, C. Diao, A. Borgna, Y. Du, Z. G. Yu, S. Pennycook, J. Xue, *Nat. Commun.* 2020, 11, 4647.

27693325, 2024, 2, Downloaded from https://onlinelibrary.wiley.com/doi/10.1002/cnl2.116 by James Cook University, Wiley Online Library on [26/11/2025]. See the Terms

conditions) on Wiley Online Library for rules

of use; OA articles are governed by the applicable Creative Commons License

- [52] R. Li, K. Xiang, Z. Peng, Y. Zou, S. Wang, Adv. Energy Mater. 2021, 11, 2102292.
- [53] N. A. Ivanova, D. D. Spasov, R. M. Mensharapov, E. V. Kukueva, A. A. Zasypkina, V. N. Fateev, S. A. Grigoriev, *Int. J. Hydrogen Energy* 2023, 48, 11410.
- [54] I. S. Pieta, A. Rathi, P. Pieta, R. Nowakowski, M. Hołdynski, M. Pisarek, A. Kaminska, M. B. Gawande, R. Zboril, Appl. Catal., B 2019, 244, 272.
- [55] D. Chen, S. D. Minteer, J. Power Sources 2015, 284, 27.
- [56] T. Take, K. Tsurutani, M. Umeda, J. Power Sources 2007, 164, 9.
- [57] S. Li, R. Ma, J. Hu, Z. Li, L. Liu, X. Wang, Y. Lu, G. E. Sterbinsky, S. Liu, L. Zheng, J. Liu, D. Liu, J. Wang, *Nat. Commun.* 2022, 13, 2916.
- [58] F. Meng, C. Dai, Z. Liu, S. Luo, J. Ge, Y. Duan, G. Chen, C. Wei, R. R. Chen, J. Wang, D. Mandler, Z. J. Xu, eScience 2022, 2, 87.
- [59] G. Han, M. Li, H. Liu, W. Zhang, L. He, F. Tian, Y. Liu, Y. Yu, W. Yang, S. Guo, Adv. Mater. 2022, 34, e2202943.
- [60] F. Si, J. Liu, Y. Zhang, B. Zhao, Y. Liang, X. Wu, X. Kang, X. Yang, J. Zhang, X. Z. Fu, J. L. Luo, Small 2023, 19, e2205257.
- [61] C. Wan, J. Jin, X. Wei, S. Chen, Y. Zhang, T. Zhu, H. Qu, J. Mater. Sci. Technol. 2022, 124, 102.
- [62] L. Zhao, Q. Sun, M. Li, Y. Zhong, P. Shen, Y. Lin, K. Xu, Sci. China Mater. 2023, 66, 1820.
- [63] Y. Hao, D. Yu, S. Zhu, C.-H. Kuo, Y.-M. Chang, L. Wang, H.-Y. Chen, M. Shao, S. Peng, *Energy Environ. Sci.* 2023, 16, 1100.
- [64] S. Rezaee, S. Shahrokhian, Appl. Catal., B 2019, 244, 802.
- [65] M. Li, X. Deng, Y. Liang, K. Xiang, D. Wu, B. Zhao, H. Yang, J.-L. Luo, X.-Z. Fu, J. Energy Chem. 2020, 50, 314.
- [66] S. Sheng, K. Ye, Y. Gao, K. Zhu, J. Yan, G. Wang, D. Cao, J. Colloid Interface Sci. 2021, 602, 325.
- [67] H. Wang, A. Guan, J. Zhang, Y. Mi, S. Li, T. Yuan, C. Jing, L. Zhang, L. Zhang, G. Zheng, Chin. J. Catal. 2022, 43, 1478.
- [68] Z. Li, S. Ning, J. Xu, J. Zhu, Z. Yuan, Y. Wu, J. Chen, F. Xie, Y. Jin, N. Wang, H. Meng, S. Sun, *Energy Environ. Sci.* 2022, 15, 5300.
- [69] Y. Zhang, W. Zhu, J. Fang, Z. Xu, Y. Xue, D. Liu, R. Sui, Q. Lv, X. Liu, Y. Wang, W. Chen, Z. Zhuang, *Nano Res.* 2021, 15, 2987.
- [70] W. Wang, Y. B. Zhu, Q. Wen, Y. Wang, J. Xia, C. Li, M. W. Chen, Y. Liu, H. Li, H. A. Wu, T. Zhai, Adv. Mater. 2019, 31, e1900528.
- [71] G.-F. Chen, Y. Luo, L.-X. Ding, H. Wang, ACS Catal. 2017, 8, 526.
- [72] V. Tournier, C. M. Topham, A. Gilles, B. David, C. Folgoas, E. Moya-Leclair, E. Kamionka, M. L. Desrousseaux, H. Texier, S. Gavalda, M. Cot, E. Guémard, M. Dalibey, J. Nomme, G. Cioci, S. Barbe, M. Chateau, I. André, S. Duquesne, A. Marty, *Nature* 2020, 580, 216.
- [73] J. Chu, Y. Cai, C. Li, X. Wang, Q. Liu, M. He, Waste Manage. 2021, 124, 273.
- [74] F. Liu, X. Gao, R. Shi, E. C. M. Tse, Y. Chen, *Green Chem.*2022, 24, 6571.
- [75] X. Liu, Z. Fang, D. Xiong, S. Gong, Y. Niu, W. Chen, Z. Chen, Nano Res. 2022, 16, 4625.
- [76] J. Wang, X. Li, T. Zhang, Y. Chen, T. Wang, Y. Zhao, J. Phys. Chem. Lett. 2022, 13, 622.

- [77] H. Zhou, Y. Ren, Z. Li, M. Xu, Y. Wang, R. Ge, X. Kong, L. Zheng, H. Duan, *Nat. Commun.* 2021, 12, 4679.
- [78] N. Wang, X. Li, M.-K. Hu, W. Wei, S.-H. Zhou, X.-T. Wu, Q.-L. Zhu, Appl. Catal., B 2022, 316, 121667.
- [79] K. Liu, Y. Wang, F. Liu, C. Liu, R. Shi, Y. Chen, Chem. Eng. J. 2023, 473, 145292.
- [80] J. Wang, X. Li, M. Wang, T. Zhang, X. Chai, J. Lu, T. Wang, Y. Zhao, D. Ma, ACS Catal. 2022, 12, 6722.
- [81] Z. Chen, R. Zheng, T. Bao, T. Ma, W. Wei, Y. Shen, B. J. Ni, Nano-Micro Lett. 2023, 15, 210.
- [82] J. Wu, X. Liu, Y. Hao, S. Wang, R. Wang, W. Du, S. Cha, X. Y. Ma, X. Yang, M. Gong, *Angew. Chem. Int. Ed.* 2023, 62, e202216083.
- [83] X. Han, H. Sheng, C. Yu, T. W. Walker, G. W. Huber, J. Qiu, S. Jin, ACS Catal. 2020, 10, 6741.
- [84] Q. Qian, X. He, Z. Li, Y. Chen, Y. Feng, M. Cheng, H. Zhang, W. Wang, C. Xiao, G. Zhang, Y. Xie, Adv. Mater. 2023, 35, e2300935.
- [85] L. Li, Z. Zhang, H. Chen, F. Chen, Nano Res. 2022, 16, 4596.
- [86] Z. He, J. Hwang, Z. Gong, M. Zhou, N. Zhang, X. Kang, J. W. Han, Y. Chen, *Nat. Commun.* 2022, 13, 3777.
- [87] Y. Wang, Y.-Q. Zhu, Z. Xie, S.-M. Xu, M. Xu, Z. Li, L. Ma, R. Ge, H. Zhou, Z. Li, X. Kong, L. Zheng, J. Zhou, H. Duan, ACS Catal. 2022, 12, 12432.
- [88] N. Xi, Y. Zang, X. Sun, J. Yu, M. Johnsson, Y. Dai, Y. Sang, H. Liu, X. Yu, Adv. Energy Mater. 2023, 13, 2301572.
- [89] Y. Zhu, Q. Qian, Y. Chen, X. He, X. Shi, W. Wang, Z. Li, Y. Feng, G. Zhang, F. Cheng, Adv. Funct. Mater. 2023, 33, 2300547.
- [90] H. Yao, Y. Wang, Y. Zheng, X. Yu, J. Ge, Y. Zhu, X. Guo, Nano Res. 2023, 16, 10832.
- [91] F. Li, C. Liu, H. Lin, Y. Sun, H. Yu, S. Xue, J. Cao, X. Jia, S. Chen, J. Colloid Interface Sci. 2023, 640, 329.
- [92] Y. Song, M. Yuan, W. Su, D. Guo, X. Chen, G. Sun, W. Zhang, *Inorg. Chem.* 2022, 61, 7308.
- [93] L. Xu, Z. Huang, M. Yang, J. Wu, W. Chen, Y. Wu, Y. Pan, Y. Lu, Y. Zou, S. Wang, *Angew. Chem. Int. Ed.* 2022, 61, e202210123.
- [94] J. Zhong, Y. Shen, P. Zhu, S. Yao, C. An, Nano Res. 2022, 16, 202.
- [95] J. Zheng, X. Chen, X. Zhong, S. Li, T. Liu, G. Zhuang, X. Li, S. Deng, D. Mei, J. G. Wang, Adv. Funct. Mater. 2017, 27, 1704169.
- [96] Y. Huang, R. Yang, G. Anandhababu, J. Xie, J. Lv, X. Zhao, X. Wang, M. Wu, Q. Li, Y. Wang, ACS Energy Lett. 2018, 3, 1854.
- [97] Y. Cao, D. Zhang, X. Kong, F. Zhang, X. Lei, J. Mater. Sci. 2021, 56, 6689.
- [98] B. You, X. Liu, X. Liu, Y. Sun, ACS Catal. 2017, 7, 4564.
- [99] Q. Xue, Z. Xia, W. Gou, J. Bu, J. Li, H. Xiao, Y. Qu, ACS Catal. 2022, 13, 400.
- [100] H. Zhou, Z. Li, S. M. Xu, L. Lu, M. Xu, K. Ji, R. Ge, Y. Yan, L. Ma, X. Kong, L. Zheng, H. Duan, *Angew. Chem. Int. Ed.* 2021, 60, 8976.
- [101] R. Li, P. Kuang, L. Wang, H. Tang, J. Yu, Chem. Eng. J. 2022, 431, 134137.
- [102] L. Ming, X.-Y. Wu, S.-S. Wang, W. Wu, C.-Z. Lu, Green Chem. 2021, 23, 7825.
- [103] Z. J. Chen, J. Dong, J. Wu, Q. Shao, N. Luo, M. Xu, Y. Sun, Y. Tang, J. Peng, H. M. Cheng, *Nat. Commun.* 2023, 14, 4210.

- [105] W. Zhou, S. Chen, X. Meng, J. Li, J. Gao, Int. J. Hydrogen Energy 2023, 48, 15748.
- [106] D. Tang, G. Lu, Z. Shen, Y. Hu, L. Yao, B. Li, G. Zhao, B. Peng, X. Huang, J. Energy Chem. 2023, 77, 80.
- [107] S. Li, D. Liu, G. Wang, P. Ma, X. Wang, J. Wang, R. Ma, Nanomicro Lett. 2023, 15, 189.
- [108] H. Chen, C. Ding, C. Kang, J. Zeng, Y. Li, Y. Li, Y. Li, C. Li, J. He, Green Chem. 2023, 25, 5320.
- [109] W. Xi, P. Yang, M. Jiang, X. Wang, H. Zhou, J. Duan, M. Ratova, D. Wu, Appl. Catal., B 2024, 341, 123291.
- [110] G. Wang, J. Chen, K. Li, J. Huang, Y. Huang, Y. Liu, X. Hu, B. Zhao, L. Yi, T. W. Jones, Z. Wen, Nano Energy 2022, 92, 106751.
- [111] S. Li, Z. Liu, L. Yang, X. Shen, Q. Liu, Z. Hu, Q. Kong, J. Ma, J. Li, H. J. Lin, C. T. Chen, X. Wang, R. Yu, Z. Wang, L. Chen, X. Yuan, A. Yan, Z. Lai, Z. Liu, Z. Yu, Z. Li, Y. Cao, S. Dong, Y. Li, S. Xiao, X. Zhang, P. Jia, S. Tian, C. Pan, F. Zeng, D. Chen, Y. Chen, J. Tang, J. Xiong, K. Jiang, X. Tan, W. Zhang, S. Zhai, T. Thundat, Z. Li, Nano Energy 2022, 98, 107335.
- [112] S. Overa, B. S. Crandall, B. Shrimant, D. Tian, B. H. Ko, H. Shin, C. Bae, F. Jiao, Nat. Catal. 2022, 5, 738.
- [113] Z. Chang, F. Kong, M. Wang, S. Han, X. Cui, H. Tian, Y. Chen, G. Meng, C. Chen, Y. Liu, Y. Huang, J. Shi, Chem Catalysis 2022, 2, 358.
- [114] S. Li, P. Ma, C. Gao, L. Liu, X. Wang, M. Shakouri, R. Chernikov, K. Wang, D. Liu, R. Ma, J. Wang, Energy Environ. Sci. 2022, 15, 3004.
- [115] J. Li, H. Li, K. Fan, J. Y. Lee, W. Xie, M. Shao, Chem Catalysis 2023, 3, 100638.
- [116] J. R. C. Junqueira, D. Das, A. Cathrin Brix, S. Dieckhöfer, J. Weidner, X. Wang, J. Shi, W. Schuhmann, ChemSusChem 2023, 16, e202202349.

AUTHOR BIOGRAPHIES



Jiawei Shi is currently a PhD candidate in the Faculty of Materials Science and Chemistry at China University of Geosciences, working in Hydrogen Energy Technology Innovation Center of Hubei Province under Prof. Weiwei Cai. His work

focuses on key material development for fuel cells and electrocatalytic upgrading of organic compounds.



Weiwei Cai is an Associate Professor in the Faculty of Materials Science and Chemistry at China University of Geosciences. Dr. Cai received his PhD degree in 2012 from Changchun Institute of Applied Chemistry, Chinese Academy of

Sciences, then joined National University of Singapore as a Research Fellow and moved to China University of Geosciences as an associate professor in 2014. His research interests mainly focus on key material development for green hydrogen production, fuel cells and electrocatalytic upgrading of organic compounds.

How to cite this article: J. Shi, J. Ma, E. Ma, J. Li, Y. Hu, L. Fan, W. Cai, Carbon Neutralization **2024**;3:285–312. https://doi.org/10.1002/cnl2.116